Performance Impact of LoS and NLoS Transmissions in Small Cell Networks

Ming Ding, *Member, IEEE*, Peng Wang, *Student Member, IEEE*, David López-Pérez, *Member, IEEE*, Guoqiang Mao, *Senior Member, IEEE*, Zihuai Lin, *Senior Member, IEEE*

arXiv:1503.04251v1 [cs.IT] 13 Mar 2015

Abstract

In this paper, we introduce a sophisticated path loss model incorporating both line-of-sight (LoS) and non-line-of-sight (NLoS) transmissions to study their performance impact in small cell networks (SCNs). Analytical results are obtained on the coverage probability and the area spectral efficiency (ASE) for two user association strategies (UASs) assuming both a general path loss model and two special cases of path loss models recommended by the 3GPP standards. The performance impact of LoS and NLoS transmissions in SCNs in terms of the coverage probability and the ASE is shown to be significant both quantitatively and qualitatively, compared with previous work that does not differentiate LoS and NLoS transmissions. Particularly, our analysis demonstrates when the density of small cells is larger than a threshold, the network coverage probability will decrease as small cells become denser, which in turn makes the ASE suffer from a slow growth or even a notable *decrease*. For practical regime of small cell density, the performance results derived from our analysis are distinctively different from previous results, and show that small cell density matters. Therefore, our results shed new insights on the design and deployment of future SCNs.

Index Terms

Stochastic geometry, Homogeneous Poisson point process (HPPP), Line-of-sight (LoS), Non-line-of-sight (NLoS), Small cell networks (SCNs), Coverage probability, Area spectral efficiency (ASE)

Ming Ding is with the National ICT Australia (NICTA) (e-mail: Ming.Ding@nicta.com.au). Peng Wang is with the School of Electrical and Information Engineering, The University of Sydney, Australia and NICTA (e-mail: thomaspeng.wang@sydney.edu.au). David López-Pérez is with Bell Labs Alcatel-Lucent, Ireland (email: dr.david.lopez@ieee.org). Guoqiang Mao is with the School of Computing and Communication, The University of Technology Sydney, Australia and NICTA (e-mail: g.mao@ieee.org). Zihuai Lin is with the School of Electrical and Information Engineering, The University of Sydney, Australia (e-mail: zihuai.lin@sydney.edu.au).

I. Introduction

Driven by a new generation of wireless user equipment (UE) and the proliferation of bandwidth-intensive applications, mobile data traffic and network load are increasing in an exponential manner, and are straining current cellular networks to a breaking point [1]. In this context, small cell networks (SCNs), comprising of remote radio heads, metrocells, picocells, femtocells and/or relay nodes, can achieve a high spatial spectrum reuse by creating a large number of small cells through network densification, which in turn can significantly enhance network capacity through exploiting cell splitting gains [2]. Due to this fact, the SCN is considered as one of the most promising approaches to rapidly increase network capacity and meet the ever-increasing capacity demands. Indeed, SCNs have attracted much momentum in the wireless communications industry and research community [2], and have also gained the attention of standardization bodies such as the 3rd Generation Partnership Project (3GPP) in the design of Long Term Evolution (LTE) networks [3].

In order to deploy SCNs in a cost-effective manner, vendors and operators need foremost a deep theoretical understanding of the implications that small cells bring about. Being aware of the need for such knowledge, the wireless industry and research community have been working relentlessly on the modeling and the analysis of the SCN deployments. However, up to know, most studies on SCNs have considered only simplistic path loss models that do not differentiate Line-of-Sight (LoS) and Non-Line-of-Sight (NLoS) transmissions [4-9].

It is well known that LoS transmission may occur when the distance between a transmitter and a receiver is small, and NLoS transmission is common in office environments and in central business districts. Furthermore, when the distance between a transmitter and a receiver decreases, the probability that an LoS path exists between them increases, thereby causing a transition from NLoS transmission to LoS transmission with a higher probability. In this light, it is of interest to study the performance impact of LoS and NLoS transmissions in SCNs, particularly dense SCNs.

Before delving deeper into the analytical study, we first implement some simulations to gain some intuitive understanding about the potential performance impact of LoS and NLoS transmissions in SCNs. Fig. 1(a) and Fig. 1(b) respectively illustrate the downlink coverage probability for SCNs with 8 small cells per macrocell and 32 small cells per macrocell, in which LoS and NLoS transmissions are not differentiated[1]. Specifically, a log-normal path loss model with a single path loss exponent

[1]The results are obtained via system-level simulations [12], and the simulation methodology and scenario are generally 3GPP-compliant. Note that in order to show the individual impact of LoS and NLoS transmissions on system performance, we make the following assumptions to simplify the 3GPP scenario: i) no shadow fading is considered, and ii) no requirement of the minimum distance between adjacent base stations is adopted. Other simulation assumptions are the same as those in [13]. Also note that the macrocells are dummy ones in the considered 3GPP SCNs.

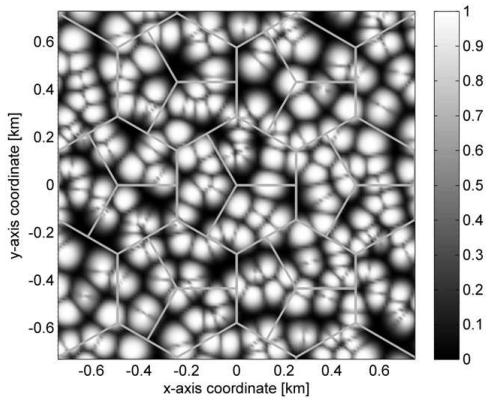

(a) Distribution of the coverage probability with a simplistic path loss model that does not differentiate LoS and NLoS transmissions (8 small cells per macrocell). The average coverage probability is 0.52.

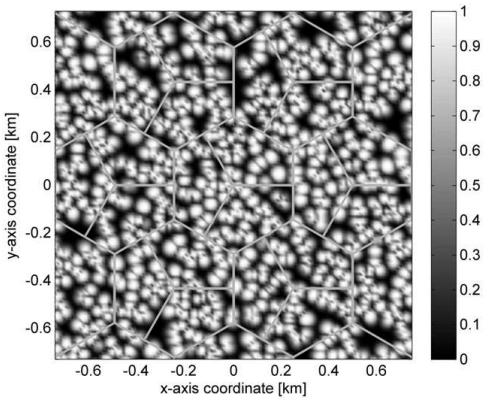

(b) Distribution of the coverage probability with a simplistic path loss model that does not differentiate LoS and NLoS transmissions (32 small cells per macrocell). The average coverage probability is 0.51.

Figure 1. Distribution of the coverage probability with a simplistic path loss model that does not differentiate LoS and NLoS transmissions. Here, the simplistic path loss model assumes a single path loss exponent. The coverage probability is defined as the probability that the corresponding signal-to-interference-plus-noise-ratio (SINR) is larger than 1. The gray-scale shading indicates the values of the coverage probabilities and higher probabilities are represented by brighter shading. Visually speaking, the sizes of the bright areas (high coverage probabilities) and the dark areas (low coverage probabilities) are approximately the same in both figures, indicating a similar performance of the average coverage probability.

is assumed. Comparing the simulation results in Fig. 1(a) and Fig. 1(b), it is easy to see that when the density of small cells increases, the performance of SCNs, measured by the downlink coverage probability, changes very little. This observation is in line with the conclusion in [4-9]. The intuition behind this phenomenon is that the increase in interference power caused by the increase in the small cell density will be almost exactly offset by the increase in signal power due to the reduced transmission distance between a UE and its associated nearest base station (BS). As a result, increasing the number of small cell BSs has little impact on the coverage probability.

However, if we run new simulations under exactly the same settings except that we adopt a path loss model incorporating both LoS and NLoS transmissions [13], it is interesting to observe that the conclusion that increasing the small cell BS density has little impact on the DL coverage probability no longer holds! Particularly, as shown in Fig. 2(a) and Fig. 2(b), assuming a path loss model incorporating both LoS and NoLS transmissions, the DL coverage probability considerably decreases from 0.35 (shown by Fig. 2(a)) to 0.24 (shown by Fig. 2(b)) when the number of small cell BSs increases from 8 to 32. This observation suggests that results on network performance obtained by assuming a simplistic path loss model that does not differentiate LoS and NLoS transmissions, may not necessarily hold when a path loss model incorporating both LoS and NLoS transmissions is considered. Therefore, LoS and NLoS transmissions that surely both occur in realistic cellular network deploymenst have a significant impact on the network performance.

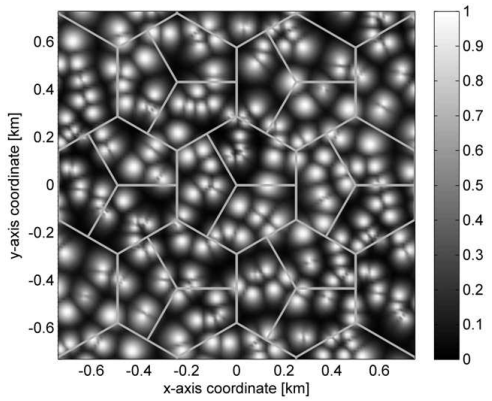

(a) Distribution of the coverage probability with a sophisticated path loss model incorporating both LoS and NLoS transmissions (8 small cells per macrocell). The average coverage probability is 0.35.

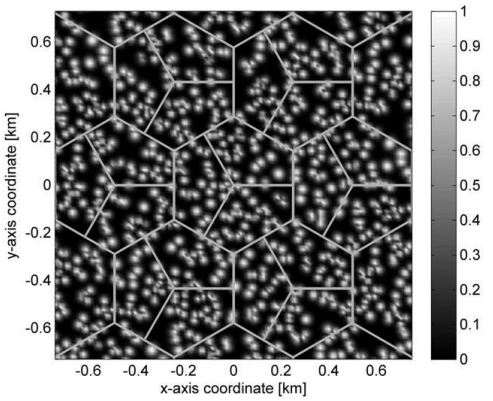

(b) Distribution of the coverage probability with a sophisticated path loss model incorporating both LoS and NLoS transmissions (32 small cells per macrocell). The average coverage probability is 0.24.

Figure 2. Distribution of the coverage probability with a sophisticated path loss model incorporating both LoS and NLoS transmissions. Here, the sophisticated path loss model is 3GPP-compliant. Visually speaking, the size of the dark areas (low coverage probabilities) in Fig. 2(b) seems to be significantly larger than that in Fig. 2(a).

This simulation-based observation motivates us to further investigate the performance impact of LoS and NLoS transmissions analytically in SCNs to gain better understanding on its implications on the design and deployment of future SCNs. The main contributions of this paper are as follows:

- Analytical results are obtained on the coverage probability and the ASE under two user association strategies (UASs) using a general path loss model incorporating both LoS and NLoS transmissions.
- Using the above results, closed-form expressions for the coverage probability and the ASE for the two UASs are further obtained for a special case, which considers the path loss model recommended by the 3GPP standards.
- Our theoretical analysis reveals an important finding, i.e., the network coverage probability will initially increase with the increase of the small cell density, but when the density of small cells is larger than a threshold, the network coverage probability will decrease as small cells become denser, which in turn makes the ASE suffer from a slow growth or even a notable *decrease*. The ASE will grow almost linearly as the small cell density increases above another larger threshold. These results are not only quantitatively but also qualitatively different from previous study results with a simplistic path loss model that does not differentiate LoS and NLoS transmissions. Thus, our study sheds valuable insights on the design and deployment of future SCNs.

The remainder of this paper is structured as follows. Section II provides a brief review on stochastic geometry and summarizes the closest related work to our work. Section III describes the system model. Section IV presents our main analytical results on the coverage probability and the ASE, followed

by their application in a 3GPP special case addressed in Section V. The derived results are validated using simulations in Section VI, with discussions shedding some new light on the performance of SCNs. Finally, the conclusions are drawn in Section VII.

II. Related Work

In stochastic geometry, small cell BS positions are typically modeled as a Homogeneous Poisson point process (HPPP) on the plane, and closed-form coverage probability expressions can be found for some scenarios in single-tier cellular networks [4-7] and multi-tier cellular networks [8-9]. The major conclusion in [4-9] is that neither the number of small cells or the number of cell tiers changes the coverage probability in interference-limited full-loaded cellular networks. However, these works consider a simplistic path loss model that does not differentiate LoS and NLoS transmissions. In contrast, in this paper, we consider a sophisticated path loss model incorporating both LoS and NLoS transmissions to study their performance impact in SCNs.

The closest related works to the one in this paper are [10] and [11]. In [10], the authors assumed a multi-slope piece-wise path loss function. Specifically, assuming that the distance between a BS and a UE is denoted by r in km, then the path loss associated with distance r in [10] is formulated as

$$\zeta\left(r\right)=\begin{cases}\zeta_1\left(r\right), & \text{when } 0\leq r\leq d_1\\ \zeta_2\left(r\right), & \text{when } d_1<r\leq d_2\\ \vdots & \vdots\\ \zeta_N\left(r\right), & \text{when } r>d_{N-1}\end{cases}, \tag{1}$$

where the path loss function $\zeta\left(r\right)$ is segmented into N pieces with each piece denoted by $\zeta_n\left(r\right)$, and $d_n, n\in\{1,2,\ldots,N-1\}$, are the segment break points.

In [11], the authors treated the event of LoS or NLoS transmission as a probabilistic event for a millimeter wave communication scenario. Specifically, the path loss associated with distance r in [11] is formulated as

$$\zeta\left(r\right) \;=\; \begin{cases}\zeta^{\mathrm{L}}\left(r\right), & \text{with probability } \mathrm{Pr}^{\mathrm{L}}\left(r\right)\\ \zeta^{\mathrm{NL}}\left(r\right), & \text{with probability } \left(1-\mathrm{Pr}^{\mathrm{L}}\left(r\right)\right)\end{cases}, \tag{2}$$

where $\zeta^{\mathrm{L}}\left(r\right)$, $\zeta^{\mathrm{NL}}\left(r\right)$ and $\mathrm{Pr}^{\mathrm{L}}\left(r\right)$ are the path loss function for the case of LoS transmission, the path loss function for the case of NLoS transmission and the LoS probability function, respectively. To simplify analysis, the LoS probability function $\mathrm{Pr}^{\mathrm{L}}\left(r\right)$ was proposed to be approximated by a moment matched equivalent step function in [11].

In [10], the multi-slope piece-wise path loss model shown in (1) does not fit well with the model defined by the 3GPP, in which the path loss function is not a one-to-one mapping to the distance.

In [11], the single-piece path loss model and the proposed step function are not compatible with the practical piece-wise path loss functions assumed in the 3GPP, the detailed modeling of which is presented in Section III. In this paper, considering the incompleteness of the works in [10] and [11], we propose a general path loss model that features piece-wise path loss functions with probabilistic LoS and NLoS transmissions.

The proposed path loss model will be formally presented in Section III. Note that the proposed model is very general and include almost all existing models used to capture LoS and NLoS transmissions [10-14] as its special cases. Furthermore, it incorporates the fact that according to some measurement studies [13], [14], the path loss function should be a piece-wise function that is better separated into several segments.

III. System Model

We consider a DL cellular network with BSs deployed in a plane according to an HPPP Φ of intensity λ BSs/km^2. UEs are Poisson distributed in the considered network with an intensity of λ^{UE} BSs/km^2. Note that λ^{UE} is assumed to be sufficiently larger than λ so that each BS has at least one associated UE in its coverage. As in (1) and (2), the distance between an arbitrary BS and an arbitrary UE is denoted by r in km. Considering practical LoS/NLoS transmissions, we propose to model the path loss associated with distance r as

$$\zeta(r) = \begin{cases} \zeta_1(r) = \begin{cases} \zeta_1^{\mathrm{L}}(r), & \text{with probability } \mathrm{Pr}_1^{\mathrm{L}}(r) \\ \zeta_1^{\mathrm{NL}}(r), & \text{with probability } \left(1-\mathrm{Pr}_1^{\mathrm{L}}(r)\right) \end{cases}, & \text{when } 0 \le r \le d_1 \\ \zeta_2(r) = \begin{cases} \zeta_2^{\mathrm{L}}(r), & \text{with probability } \mathrm{Pr}_2^{\mathrm{L}}(r) \\ \zeta_2^{\mathrm{NL}}(r), & \text{with probability } \left(1-\mathrm{Pr}_2^{\mathrm{L}}(r)\right) \end{cases}, & \text{when } d_1 < r \le d_2 \\ \vdots & & \vdots \\ \zeta_N(r) = \begin{cases} \zeta_N^{\mathrm{L}}(r), & \text{with probability } \mathrm{Pr}_N^{\mathrm{L}}(r) \\ \zeta_N^{\mathrm{NL}}(r), & \text{with probability } \left(1-\mathrm{Pr}_N^{\mathrm{L}}(r)\right) \end{cases}, & \text{when } r > d_{N-1} \end{cases}, \quad (3)$$

where the path loss function $\zeta(r)$ is segmented into N pieces with each piece denoted by $\zeta_n(r)$. Besides, $\zeta_n^{\mathrm{L}}(r)$, $\zeta_n^{\mathrm{NL}}(r)$ and $\mathrm{Pr}_n^{\mathrm{L}}(r), n \in \{1,2,\ldots,N\}$, are the n-th piece of path loss function for LoS transmission, the n-th piece of path loss function for NLoS transmission, and the n-th piece of the LoS probability function, respectively. This is a very general model, which includes almost all existing models used to capture probabilistic LoS and NLoS transmissions [13], [14] as its special cases.

Furthermore, $\zeta_n^{\mathrm{L}}(r)$ and $\zeta_n^{\mathrm{NL}}(r)$ are modeled as

$$\zeta_n(r) = \begin{cases} \zeta_n^{\mathrm{L}}(r) = A_n^{\mathrm{L}} r^{-\alpha_n^{\mathrm{L}}}, & \text{for LoS} \\ \zeta_n^{\mathrm{NL}}(r) = A_n^{\mathrm{NL}} r^{-\alpha_n^{\mathrm{NL}}}, & \text{for NLoS} \end{cases}, \tag{4}$$

where A_n^{L} and $A_n^{\mathrm{NL}}, n \in \{1, 2, \ldots, N\}$ are the path losses at a reference distance $r = 1$ for the LoS and the NLoS cases in $\zeta_n(r)$, respectively, and α_n^{L} and $\alpha_n^{\mathrm{NL}}, n \in \{1, 2, \ldots, N\}$ are the path loss exponents for the LoS and the NLoS cases in $\zeta_n(r)$, respectively. In practice, A_n^{L}, A_n^{NL}, α_n^{L} and α_n^{NL} are constants obtained from field tests [13], [14].

Finally, in (3), $\mathrm{Pr}_n^{\mathrm{L}}(r)$ is the n-th piece probability function that a transmitter and a receiver separated by a distance r has an LoS path, which is typically a monotonically decreasing function with respect to r. For convenience, $\left\{\mathrm{Pr}_n^{\mathrm{L}}(r)\right\}$ is further stacked into a piece-wise LoS probability function expressed as

$$\mathrm{Pr}^{\mathrm{L}}(r) = \begin{cases} \mathrm{Pr}_1^{\mathrm{L}}(r), & \text{when } 0 \le r \le d_1 \\ \mathrm{Pr}_2^{\mathrm{L}}(r), & \text{when } d_1 < r \le d_2 \\ \vdots & \vdots \\ \mathrm{Pr}_N^{\mathrm{L}}(r), & \text{when } r > d_{N-1} \end{cases}. \tag{5}$$

Our model is consistent with the one adopted in the 3GPP [13], [14]. Obviously, the considered path loss model will degenerate to that addressed in [10] and [11] when $\mathrm{Pr}_n^{\mathrm{L}}(r) = 0, \forall n \in \{1, 2, \ldots, N\}$ and $N = 1$, respectively.

As a common practice in the field [4-10], the multi-path fading between an arbitrary BS and an arbitrary UE is modeled as independently identical distributed (i.i.d.) Rayleigh fading. Specifically, the channel gain is denoted by h and is modeled as an i.i.d. exponential random variable (RV). We further denote by P and N_0 the transmit power of each BS and the additive white Gaussian noise (AWGN) power at each UE, respectively.

Furthermore, in this paper, we consider two user association strategies (UASs), which are

- *UAS 1*: Each UE is associated with the BS with the smallest path loss to the UE [11], [16]
- *UAS 2*: Each UE is associated with the nearest BS to the UE [4], [10]

Provided that all small cell BSs transmit with the same power, UAS 1 implies a strategy that associates each UE to the BS with the strongest signal reception strength, averaging out the multi-path fading. Using UAS 1, it is possible for a UE to associate with a BS further way but with an LoS path, instead of a nearest BS with an NLoS path. Note that both association strategies are widely used in the literature [4], [10], [11], [16].

IV. Analysis Based on the General Path Loss Model

Using the properties of the Poisson point process, we study the performance of SCNs by considering the performance of a typical UE located at the origin o. We first investigate the coverage probability that the typical UE is covered by its associated BS. The coverage probability is defined as the probability that the signal to interference plus noise ratio (SINR), denoted by SINR, is above a per-designated threshold γ:

$$p^{\mathrm{cov}}(\lambda,\gamma) = \Pr[\mathrm{SINR} > \gamma], \tag{6}$$

where the SINR is computed by

$$\mathrm{SINR} = \frac{P\zeta(r)h}{I_r + N_0}, \tag{7}$$

where I_r is the cumulative interference given by

$$I_r = \sum_{i\in\Phi/b_o} P\beta_i g_i, \tag{8}$$

where b_o is the BS associated with the typical UE and located at distance r from the typical UE, and β_i and g_i are the path loss and the multi-path fading channel gain associated with the i-th interfering BS, respectively.

Moreover, according to [10] and [11], the area spectral efficiency (ASE) in bps/Hz/km^2 for a given λ can be expressed as

$$A^{\mathrm{ASE}}(\lambda,\gamma_0) = \lambda\int_{\gamma_0}^{\infty}\log_2(1+x)\,f_X(\lambda,x)\,dx, \tag{9}$$

where γ_0 is the minimum working SINR for the considered SCN, and $f_X(\lambda,x)$ is the probability density function (PDF) of SINR observed at the typical UE at a particular value of λ.

Based on the definition of $p^{\mathrm{cov}}(\lambda,\gamma)$, which is the complementary cumulative distribution function (CCDF) of SINR, $f_X(\lambda,x)$ can be computed by

$$f_X(\lambda,x) = \frac{\partial\left(1-p^{\mathrm{cov}}(\lambda,x)\right)}{\partial x}. \tag{10}$$

Given the definition of the coverage probability and the ASE respectively presented in (6) and (9), in the following we will analyze the two performance measures for the two UASs.

A. Analysis for UAS 1

Based on the path loss model of (3), we present our main result on $p^{\mathrm{cov}}(\lambda,\gamma)$ for UAS 1 in Theorem 1.

Theorem 1. *Considering the path loss model of (3) and UAS 1, $p^{\mathrm{cov}}(\lambda,\gamma)$ can be derived as*

$$p^{cov}(\lambda,\gamma) = \sum_{n=1}^{N}\left(T_n^L + T_n^{NL}\right), \tag{11}$$

where $T_n^L = \int_{d_{n-1}}^{d_n} Pr\left[\frac{P\zeta_n^L(r)h}{I_r+N_0} > \gamma\right] f_{R,n}^L(r)\,dr$, $T_n^{NL} = \int_{d_{n-1}}^{d_n} Pr\left[\frac{P\zeta_n^{NL}(r)h}{I_r+N_0} > \gamma\right] f_{R,n}^{NL}(r)\,dr$, *and* d_0 *and* d_N *are respectively defined as* 0 *and* ∞. *Moreover,* $f_{R,n}^L(r)$ *and* $f_{R,n}^{NL}(r)$ *are represented as*

$$\begin{aligned} f_{R,n}^L(r) &= \exp\left(-\int_0^{r_1}\left(1-Pr^L(u)\right)2\pi u\lambda du\right)\times\exp\left(-\int_0^{r}Pr^L(u)\,2\pi u\lambda du\right) \\ &\quad \times Pr_n^L(r)\times 2\pi r\lambda, \quad (d_{n-1}<r\le d_n), \end{aligned} \tag{12}$$

and

$$\begin{aligned} f_{R,n}^{NL}(r) &= \exp\left(-\int_0^{r_2}Pr^L(u)\,2\pi u\lambda du\right)\times\exp\left(-\int_0^{r}\left(1-Pr^L(u)\right)2\pi u\lambda du\right) \\ &\quad \times\left(1-Pr_n^L(r)\right)\times 2\pi r\lambda, \quad (d_{n-1}<r\le d_n), \end{aligned} \tag{13}$$

where r_1 *and* r_2 *are determined by the value of* r *and given implicitly in the following equations as*

$$\zeta_n^{NL}(r_1) = \zeta_n^L(r), \tag{14}$$

and

$$\zeta_n^L(r_2) = \zeta_n^{NL}(r). \tag{15}$$

Furthermore, $Pr\left[\frac{P\zeta_n^L(r)h}{I_r+N_0} > \gamma\right]$ *and* $Pr\left[\frac{P\zeta_n^{NL}(r)h}{I_r+N_0} > \gamma\right]$ *are respectively computed by*

$$Pr\left[\frac{P\zeta_n^L(r)\,h}{I_r+N_0} > \gamma\right] = \exp\left(-\frac{\gamma N_0}{P\zeta_n^L(r)}\right)\mathscr{L}_{I_r}\left(\frac{\gamma}{P\zeta_n^L(r)}\right), \tag{16}$$

and

$$Pr\left[\frac{P\zeta_n^{NL}(r)\,h}{I_r+N_0} > \gamma\right] = \exp\left(-\frac{\gamma N_0}{P\zeta_n^{NL}(r)}\right)\mathscr{L}_{I_r}\left(\frac{\gamma}{P\zeta_n^{NL}(r)}\right), \tag{17}$$

where $\mathscr{L}_{I_r}(s)$ *is the Laplace transform of RV* I_r *evaluated at* s.

Proof: See Appendix A. ■

Plugging $p^{\text{cov}}(\lambda,\gamma)$ obtained from (11) into (10) , we can get the result of ASE from (9) for UAS 1.

As can be observed from Theorem 1, the piece-wise path loss function for LoS transmission $\left\{\zeta_n^{\text{L}}(r)\right\}$, the piece-wise path loss function for NLoS transmission $\left\{\zeta_n^{\text{NL}}(r)\right\}$, and the piece-wise LoS probability function $\left\{\text{Pr}_n^{\text{L}}(r)\right\}$ play active roles in determining the final result of $p^{\text{cov}}(\lambda,\gamma)$. We will investigate their impacts on network performance in detail in the following sections.

B. Coverage Analysis for UAS 2

Based on the path loss model of (3), we present our main result on $p^{\text{cov}}(\lambda,\gamma)$ for UAS 2 in Theorem 2.

Theorem 2. *Considering the path loss model of (3) and UAS 2, $p^{cov}(\lambda,\gamma)$ can be derived as*

$$p^{cov}(\lambda,\gamma) = \sum_{n=1}^{N}\left(T_n^L + T_n^{NL}\right), \tag{18}$$

where $T_n^L = \int_{d_{n-1}}^{d_n} Pr\left[\frac{P\zeta_n^L(r)h}{I_r+N_0} > \gamma\right] f_{R,n}^L(r)\,dr$, $T_n^{NL} = \int_{d_{n-1}}^{d_n} Pr\left[\frac{P\zeta_n^{NL}(r)h}{I_r+N_0} > \gamma\right] f_{R,n}^{NL}(r)\,dr$, and d_0 and d_N are respectively defined as 0 and ∞. Moreover, $f_{R,n}^L(r)$ and $f_{R,n}^{NL}(r)$ are represented as

$$f_{R,n}^L(r) = Pr_n^L(r)\times\exp\left(-\pi r^2\lambda\right)\times 2\pi r\lambda, \quad (d_{n-1}<r\le d_n), \tag{19}$$

and

$$f_{R,n}^{NL}(r) = \left(1-Pr_n^L(r)\right)\times\exp\left(-\pi r^2\lambda\right)\times 2\pi r\lambda, \quad (d_{n-1}<r\le d_n). \tag{20}$$

Furthermore, $Pr\left[\frac{P\zeta_n^L(r)h}{I_r+N_0} > \gamma\right]$ and $Pr\left[\frac{P\zeta_n^{NL}(r)h}{I_r+N_0} > \gamma\right]$ are respectively computed by

$$Pr\left[\frac{P\zeta_n^L(r)\,h}{I_r+N_0} > \gamma\right] = \exp\left(-\frac{\gamma N_0}{P\zeta_n^L(r)}\right)\mathscr{L}_{I_r}\left(\frac{\gamma}{P\zeta_n^L(r)}\right), \tag{21}$$

and

$$Pr\left[\frac{P\zeta_n^{NL}(r)\,h}{I_r+N_0} > \gamma\right] = \exp\left(-\frac{\gamma N_0}{P\zeta_n^{NL}(r)}\right)\mathscr{L}_{I_r}\left(\frac{\gamma}{P\zeta_n^{NL}(r)}\right), \tag{22}$$

where $\mathscr{L}_{I_r}(s)$ is the Laplace transform of RV I_r evaluated at s.

Proof: See Appendix B. ■

Plugging $p^{\text{cov}}(\lambda,\gamma)$ obtained from (18) into (10), we can get the result of ASE from (9) for UAS 2.

A similar observation as that in Theorem 1 can be drawn for Theorem 2, i.e., the final result of $p^{\text{cov}}(\lambda,\gamma)$ is also affected by the piece-wise functions $\left\{\zeta_n^{\text{L}}(r)\right\}$, $\left\{\zeta_n^{\text{NL}}(r)\right\}$, and $\left\{\text{Pr}_n^{\text{L}}(r)\right\}$. We will investigate the analytical results in detail in the following sections.

V. Study of a 3GPP Special Case

As a special case of Theorem 1 and Theorem 2, we consider the path loss function, $\zeta(r)$, adopted in the 3GPP as [13]

$$\zeta(r) = \begin{cases} A^{\text{L}} r^{-\alpha^{\text{L}}}, & \text{with probability } \text{Pr}^{\text{L}}(r) \\ A^{\text{NL}} r^{-\alpha^{\text{NL}}}, & \text{with probability } \left(1-\text{Pr}^{\text{L}}(r)\right) \end{cases}, \tag{23}$$

together with the linear LoS probability function, $\text{Pr}^{\text{L}}(r)$, defined in the 3GPP as [14]

$$\text{Pr}^{\text{L}}(r) = \begin{cases} 1-\frac{r}{d_1}, & 0<r\le d_1 \\ 0, & r>d_1 \end{cases}. \tag{24}$$

Considering the general path loss model presented in (3), the path loss model presented in (23) and (24) can be deemed as a special case of (3) with the following substitution: $N=2$, $\zeta_1^{\text{L}}(r)=\zeta_2^{\text{L}}(r)=$

$A^{\mathrm{L}}r^{-\alpha^{\mathrm{L}}}$, $\zeta_1^{\mathrm{NL}}(r)=\zeta_2^{\mathrm{NL}}(r)=A^{\mathrm{NL}}r^{-\alpha^{\mathrm{NL}}}$, $\mathrm{Pr}_1^{\mathrm{L}}(r)=1-\frac{r}{d_1}$, and $\mathrm{Pr}_2^{\mathrm{L}}(r)=0$. For clarity, this 3GPP special case is referred to as 3GPP case 1 in the sequel.

A. Analysis for UAS 1 in 3GPP Case 1

According to Theorem 1, $p^{\mathrm{cov}}(\lambda,\gamma)$ for UAS 1 can then be obtained as

$$p^{\mathrm{cov}}(\lambda,\gamma) = \sum_{n=1}^{2}\left(T_n^{\mathrm{L}}+T_n^{\mathrm{NL}}\right). \tag{25}$$

In the following sections, we investigate T_1^{L}, T_1^{NL}, T_2^{L}, and T_2^{NL}, respectively.

1) The Computation of T_1^L: From Theorem 1, T_1^{L} for UAS 1 can be obtained as

$$\begin{aligned} T_1^{\mathrm{L}} &= \int_0^{d_1}\exp\left(-\frac{\gamma N_0}{P\zeta_1^{\mathrm{L}}(r)}\right)\mathscr{L}_{I_r}\left(\frac{\gamma}{P\zeta_1^{\mathrm{L}}(r)}\right)f_{R,1}^{\mathrm{L}}(r)\,dr \\ &\overset{(a)}{=} \int_0^{d_1}\exp\left(-\frac{\gamma r^{\alpha^{\mathrm{L}}}N_0}{PA^{\mathrm{L}}}\right)\mathscr{L}_{I_r}\left(\frac{\gamma r^{\alpha^{\mathrm{L}}}}{PA^{\mathrm{L}}}\right)f_{R,1}^{\mathrm{L}}(r)\,dr, \end{aligned} \tag{26}$$

where $\zeta_1^{\mathrm{L}}(r)=A^{\mathrm{L}}r^{-\alpha^{\mathrm{L}}}$ from (23) is plugged into (a) of (26) and $\mathscr{L}_{I_r}(s)$ is the Laplace transform of RV I_r evaluated at s.

For UAS 1, according to Theorem 1 and (24), $f_{R,1}^{\mathrm{L}}(r)$ can be derived as

$$\begin{aligned} f_{R,1}^{\mathrm{L}}(r) &= \exp\left(-\int_0^{r_1}\lambda\frac{u}{d_1}2\pi u du\right)\times\exp\left(-\int_0^{r}\lambda\left(1-\frac{u}{d_1}\right)2\pi u du\right)\times\left(1-\frac{r}{d_1}\right)\times 2\pi r\lambda \\ &= \exp\left(-\pi\lambda r^2+2\pi\lambda\left(\frac{r^3}{3d_1}-\frac{r_1^3}{3d_1}\right)\right)\times\left(1-\frac{r}{d_1}\right)\times 2\pi r\lambda, \quad (0<r\le d_1), \end{aligned} \tag{27}$$

where $r_1=\left(\frac{A^{\mathrm{NL}}}{A^{\mathrm{L}}}\right)^{\frac{1}{\alpha^{\mathrm{NL}}}}r^{\frac{\alpha^{\mathrm{L}}}{\alpha^{\mathrm{NL}}}}$ according to (14).

Besides, to compute $\mathscr{L}_{I_r}\left(\frac{\gamma r^{\alpha^{\mathrm{L}}}}{PA^{\mathrm{L}}}\right)$ for UAS 1 in the range of $0<r\le d_1$, we propose Lemma 3.

Lemma 3. *$\mathscr{L}_{I_r}\left(\frac{\gamma r^{\alpha^{\mathrm{L}}}}{PA^{\mathrm{L}}}\right)$ for UAS 1 in the range of $0<r\le d_1$ can be calculated by*
$\mathscr{L}_{I_r}\left(\frac{\gamma r^{\alpha^{\mathrm{L}}}}{PA^{\mathrm{L}}}\right)$ =

$$\begin{aligned} &\exp\left(-2\pi\lambda\left(\rho_1\left(\alpha^{\mathrm{L}},1,\left(\gamma r^{\alpha^{\mathrm{L}}}\right)^{-1},d_1\right)-\rho_1\left(\alpha^{\mathrm{L}},1,\left(\gamma r^{\alpha^{\mathrm{L}}}\right)^{-1},r\right)\right)\right) \\ &\times\exp\left(\frac{2\pi\lambda}{d_0}\left(\rho_1\left(\alpha^{\mathrm{L}},2,\left(\gamma r^{\alpha^{\mathrm{L}}}\right)^{-1},d_1\right)-\rho_1\left(\alpha^{\mathrm{L}},2,\left(\gamma r^{\alpha^{\mathrm{L}}}\right)^{-1},r\right)\right)\right) \\ &\times\exp\left(-\frac{2\pi\lambda}{d_0}\left(\rho_1\left(\alpha^{\mathrm{NL}},2,\left(\frac{\gamma A^{\mathrm{NL}}}{A^{\mathrm{L}}}r^{\alpha^{\mathrm{L}}}\right)^{-1},d_1\right)-\rho_1\left(\alpha^{\mathrm{NL}},2,\left(\frac{\gamma A^{\mathrm{NL}}}{A^{\mathrm{L}}}r^{\alpha^{\mathrm{L}}}\right)^{-1},r_1\right)\right)\right) \\ &\times\exp\left(-2\pi\lambda\rho_2\left(\alpha^{\mathrm{NL}},1,\left(\frac{\gamma A^{\mathrm{NL}}}{A^{\mathrm{L}}}r^{\alpha^{\mathrm{L}}}\right)^{-1},d_1\right)\right), \quad (0<r\le d_1) \end{aligned} \tag{28}$$

where

$$\rho_1(\alpha,\beta,t,d) = \left[\frac{d^{(\beta+1)}}{\beta+1}\right] {}_2F_1\left[1,\frac{\beta+1}{\alpha};1+\frac{\beta+1}{\alpha};-td^{\alpha}\right], \quad (29)$$

and

$$\rho_2(\alpha,\beta,t,d) = \left[\frac{d^{-(\alpha-\beta-1)}}{t(\alpha-\beta-1)}\right] {}_2F_1\left[1,1-\frac{\beta+1}{\alpha};2-\frac{\beta+1}{\alpha};-\frac{1}{td^{\alpha}}\right], (\alpha>\beta+1), \quad (30)$$

where ${}_2F_1[\cdot,\cdot;\cdot;\cdot]$ *is the hyper-geometric function [15].*

Proof: See Appendix C. ■

To sum up, for UAS 1, T_1^{L} can be evaluated as

$$T_1^{\mathrm{L}} = \int_0^{d_1} \exp\left(-\frac{\gamma r^{\alpha^{\mathrm{L}}} N_0}{PA^{\mathrm{L}}}\right) \mathscr{L}_{I_r}\left(\frac{\gamma r^{\alpha^{\mathrm{L}}}}{PA^{\mathrm{L}}}\right) f_{R,1}^{\mathrm{L}}(r)\, dr, \quad (31)$$

where $f_{R,1}^{\mathrm{L}}(r)$ and $\mathscr{L}_{I_r}\left(\frac{\gamma r^{\alpha^{\mathrm{L}}}}{PA^{\mathrm{L}}}\right)$ are computed by (27) and (28), respectively.

2) The Computation of T_1^{NL}: From Theorem 1, T_1^{NL} for UAS 1 can be obtained as

$$\begin{aligned} T_1^{\mathrm{NL}} &= \int_0^{d_1} \exp\left(-\frac{\gamma N_0}{P\zeta_1^{\mathrm{NL}}(r)}\right) \mathscr{L}_{I_r}\left(\frac{\gamma}{P\zeta_1^{\mathrm{NL}}(r)}\right) f_{R,1}^{\mathrm{NL}}(r)\, dr \\ &\overset{(a)}{=} \int_0^{d_1} \exp\left(-\frac{\gamma r^{\alpha^{\mathrm{NL}}} N_0}{PA^{\mathrm{NL}}}\right) \mathscr{L}_{I_r}\left(\frac{\gamma r^{\alpha^{\mathrm{NL}}}}{PA^{\mathrm{NL}}}\right) f_{R,1}^{\mathrm{NL}}(r)\, dr, \end{aligned} \quad (32)$$

where $\zeta_1^{\mathrm{NL}}(r) = A^{\mathrm{NL}} r^{-\alpha^{\mathrm{NL}}}$ from (23) is plugged into (a) of (32) and $\mathscr{L}_{I_r}(s)$ is the Laplace transform of RV I_r evaluated at s.

For UAS 1, according to Theorem 1 and (24), $f_{R,1}^{\mathrm{NL}}(r)$ can be written as

$$\begin{aligned} f_{R,1}^{\mathrm{NL}}(r) &= \exp\left(-\int_0^{r_2} \lambda \mathrm{Pr}^{\mathrm{L}}(u)\, 2\pi u du\right) \\ &\quad \times \exp\left(-\int_0^{r} \lambda\left(1-\mathrm{Pr}^{\mathrm{L}}(u)\right) 2\pi u du\right) \times \frac{r}{d_1} \times 2\pi r\lambda, \quad (0<r\le d_1), \end{aligned} \quad (33)$$

where $r_2 = \left(\frac{A^{\mathrm{L}}}{A^{\mathrm{NL}}}\right)^{\frac{1}{\alpha^{\mathrm{L}}}} r^{\frac{\alpha^{\mathrm{NL}}}{\alpha^{\mathrm{L}}}}$ according to (15). Since the numerical relationship between r_2 and d_1 affects the calculation of the first multiplier in (33), i.e., $\exp\left(-\int_0^{r_2} \lambda \mathrm{Pr}^{\mathrm{L}}(u)\, 2\pi u du\right)$, we will discuss the cases of $0<r_2\le d_1$ and $r_2>d_1$ in the following.

If $0<r_2\le d_1$, i.e., $0<r\le x_1 = d_1^{\frac{\alpha^{\mathrm{L}}}{\alpha^{\mathrm{NL}}}} \left(\frac{A^{\mathrm{NL}}}{A^{\mathrm{L}}}\right)^{\frac{1}{\alpha^{\mathrm{NL}}}}$, we have

$$\begin{aligned} f_{R,1}^{\mathrm{NL}}(r) &= \exp\left(-\int_0^{r_2} \lambda\left(1-\frac{u}{d_1}\right) 2\pi u du\right) \times \exp\left(-\int_0^{r} \lambda\frac{u}{d_1} 2\pi u du\right) \times \frac{r}{d_1} \times 2\pi r\lambda \\ &= \exp\left(-\pi\lambda r_2^2 + 2\pi\lambda\left(\frac{r_2^3}{3d_1} - \frac{r^3}{3d_1}\right)\right) \times \left(\frac{r}{d_1}\right) \times 2\pi r\lambda, \quad (0<r\le x_1). \end{aligned} \quad (34)$$

Otherwise, if $r_2>d_1$, i.e., $x_1<r\le d_1$, we can get

$$f_{R,1}^{\mathrm{NL}}(r) = \exp\left(-\int_0^{d_1}\lambda\left(1-\frac{u}{d_1}\right)2\pi u du\right)\times\exp\left(-\int_0^{r}\lambda\frac{u}{d_1}2\pi u du\right)\times\frac{r}{d_1}\times 2\pi r\lambda$$
$$= \exp\left(-\frac{\pi\lambda d_1^2}{3}-\frac{2\pi\lambda r^3}{3d_1}\right)\times\left(\frac{r}{d_1}\right)\times 2\pi r\lambda, \quad (x_1 < r \le d_1). \tag{35}$$

Besides, to compute $\mathscr{L}_{I_r}\left(\frac{\gamma r^{\alpha^{\mathrm{NL}}}}{PA^{\mathrm{NL}}}\right)$ for UAS 1 in the range of $0 < r \le d_1$, we propose Lemma 4. Note that since the calculation of $f_{R,1}^{\mathrm{NL}}(r)$ is divided into two cases, i.e., $0 < r \le x_1$ and $x_1 < r \le d_1$, the calculation of $\mathscr{L}_{I_r}\left(\frac{\gamma r^{\alpha^{\mathrm{NL}}}}{PA^{\mathrm{NL}}}\right)$ for UAS 1 in the range of $0 < r \le d_1$ will also be divided into those cases, because the interference in $\mathscr{L}_{I_r}\left(\frac{\gamma r^{\alpha^{\mathrm{NL}}}}{PA^{\mathrm{NL}}}\right)$ needs to be integrated from the distance r to infinity.

Lemma 4. *$\mathscr{L}_{I_r}\left(\frac{\gamma r^{\alpha^{\mathrm{NL}}}}{PA^{\mathrm{NL}}}\right)$ for UAS 1 in the range of $0 < r \le d_1$ can be divided for two cases, i.e., $0 < r \le x_1$ and $x_1 < r \le d_1$. The results are as follows,*

$\mathscr{L}_{I_r}\left(\frac{\gamma r^{\alpha^{\mathrm{NL}}}}{PA^{\mathrm{NL}}}\right) =$

$$\exp\left(-2\pi\lambda\left(\rho_1\left(\alpha^{\mathrm{L}},1,\left(\frac{\gamma A^{\mathrm{L}}}{A^{\mathrm{NL}}}r^{\alpha^{\mathrm{NL}}}\right)^{-1},d_1\right)-\rho_1\left(\alpha^{\mathrm{L}},1,\left(\frac{\gamma A^{\mathrm{L}}}{A^{\mathrm{NL}}}r^{\alpha^{\mathrm{NL}}}\right)^{-1},r_2\right)\right)\right)$$
$$\times\exp\left(\frac{2\pi\lambda}{d_0}\left(\rho_1\left(\alpha^{\mathrm{L}},2,\left(\frac{\gamma A^{\mathrm{L}}}{A^{\mathrm{NL}}}r^{\alpha^{\mathrm{NL}}}\right)^{-1},d_1\right)-\rho_1\left(\alpha^{\mathrm{L}},2,\left(\frac{\gamma A^{\mathrm{L}}}{A^{\mathrm{NL}}}r^{\alpha^{\mathrm{NL}}}\right)^{-1},r_2\right)\right)\right)$$
$$\times\exp\left(-\frac{2\pi\lambda}{d_0}\left(\rho_1\left(\alpha^{\mathrm{NL}},2,\left(\gamma r^{\alpha^{\mathrm{NL}}}\right)^{-1},d_1\right)-\rho_1\left(\alpha^{\mathrm{NL}},2,\left(\gamma r^{\alpha^{\mathrm{NL}}}\right)^{-1},r\right)\right)\right)$$
$$\times\exp\left(-2\pi\lambda\rho_2\left(\alpha^{\mathrm{NL}},1,\left(\gamma r^{\alpha^{\mathrm{NL}}}\right)^{-1},d_1\right)\right), \quad (0 < r \le x_1), \tag{36}$$

and

$$\mathscr{L}_{I_r}\left(\frac{\gamma r^{\alpha^{\mathrm{NL}}}}{PA^{\mathrm{NL}}}\right) = \exp\left(-\frac{2\pi\lambda}{d_0}\left(\rho_1\left(\alpha^{\mathrm{NL}},2,\left(\gamma r^{\alpha^{\mathrm{NL}}}\right)^{-1},d_1\right)-\rho_1\left(\alpha^{\mathrm{NL}},2,\left(\gamma r^{\alpha^{\mathrm{NL}}}\right)^{-1},r\right)\right)\right)$$
$$\times\exp\left(-2\pi\lambda\rho_2\left(\alpha^{\mathrm{NL}},1,\left(\gamma r^{\alpha^{\mathrm{NL}}}\right)^{-1},d_1\right)\right), \quad (x_1 < r \le d_1), \tag{37}$$

where $\rho_1(\alpha,\beta,t,d)$ and $\rho_2(\alpha,\beta,t,d)$ are defined in (29) and (30), respectively.

Proof: See Appendix D. ∎

To sum up, for UAS 1, T_1^{NL} can be evaluated as

$$T_1^{\mathrm{NL}} = \int_0^{x_1}\exp\left(-\frac{\gamma r^{\alpha^{\mathrm{NL}}}N_0}{PA^{\mathrm{NL}}}\right)\left[\mathscr{L}_{I_r}\left(\frac{\gamma r^{\alpha^{\mathrm{NL}}}}{PA^{\mathrm{NL}}}\right)f_{R,1}^{\mathrm{NL}}(r)\middle| 0 < r \le x_1\right]dr$$
$$+\int_{x_1}^{d_1}\exp\left(-\frac{\gamma r^{\alpha^{\mathrm{NL}}}N_0}{PA^{\mathrm{NL}}}\right)\left[\mathscr{L}_{I_r}\left(\frac{\gamma r^{\alpha^{\mathrm{NL}}}}{PA^{\mathrm{NL}}}\right)f_{R,1}^{\mathrm{NL}}(r)\middle| x_1 < r \le d_1\right]dr, \tag{38}$$

where $f_{R,1}^{\mathrm{NL}}(r)$ is computed by (34) and (35), and $\mathscr{L}_{I_r}\left(\frac{\gamma r^{\alpha^{\mathrm{NL}}}}{PA^{\mathrm{NL}}}\right)$ is given by (36) and (37).

3) The Computation of T_2^{L}: From Theorem 1, T_2^{L} for UAS 1 can be derived as

$$T_2^{\mathrm{L}} = \int_{d_1}^{\infty} \exp\left(-\frac{\gamma N_0}{P\zeta_2^{\mathrm{L}}(r)}\right) \mathscr{L}_{I_r}\left(\frac{\gamma}{P\zeta_2^{\mathrm{L}}(r)}\right) f_{R,2}^{\mathrm{L}}(r)\, dr. \tag{39}$$

For UAS 1, according to Theorem 1 and (24), $f_{R,1}^{\mathrm{NL}}(r)$ can be calculated by

$$\begin{aligned} f_{R,2}^{\mathrm{L}}(r) &= \exp\left(-\int_0^{r_1} \lambda\left(1-\mathrm{Pr}^{\mathrm{L}}(u)\right) 2\pi u du\right) \times \exp\left(-\int_0^{r} \lambda \mathrm{Pr}^{\mathrm{L}}(u)\, 2\pi u du\right) \times 0 \times 2\pi r\lambda \\ &= 0, \quad (r > d_1). \end{aligned} \tag{40}$$

Plugging (40) into (39), yields

$$T_2^{\mathrm{L}} = 0. \tag{41}$$

4) The Computation of T_2^{NL}: From Theorem 1, T_2^{NL} for UAS 1 can be derived as

$$\begin{aligned} T_2^{\mathrm{NL}} &= \int_{d_1}^{\infty} \exp\left(-\frac{\gamma N_0}{P\zeta_2^{\mathrm{NL}}(r)}\right) \mathscr{L}_{I_r}\left(\frac{\gamma}{P\zeta_2^{\mathrm{NL}}(r)}\right) f_{R,2}^{\mathrm{NL}}(r)\, dr \\ &\overset{(a)}{=} \int_{d_1}^{\infty} \exp\left(-\frac{\gamma r^{\alpha^{\mathrm{NL}}} N_0}{PA^{\mathrm{NL}}}\right) \mathscr{L}_{I_r}\left(\frac{\gamma r^{\alpha^{\mathrm{NL}}}}{PA^{\mathrm{NL}}}\right) f_{R,2}^{\mathrm{NL}}(r)\, dr, \end{aligned} \tag{42}$$

where $\zeta_2^{\mathrm{NL}}(r) = A^{\mathrm{NL}} r^{-\alpha^{\mathrm{NL}}}$ from (23) is plugged into (a) of (42) and $\mathscr{L}_{I_r}(s)$ is the Laplace transform of RV I_r evaluated at s.

For UAS 1, according to Theorem 1 and (24), $f_{R,2}^{\mathrm{NL}}(r)$ can be derived as

$$\begin{aligned} f_{R,2}^{\mathrm{NL}}(r) &= \exp\left(-\int_0^{d_1} \lambda\left(1-\frac{u}{d_1}\right) 2\pi u du\right) \times \exp\left(-\int_0^{d_1} \lambda \frac{u}{d_1} 2\pi u du - \int_{d_1}^{r} \lambda 2\pi u du\right) \times 2\pi r\lambda \\ &= \exp\left(-\pi\lambda r^2\right) \times 2\pi r\lambda, \quad (r > d_1). \end{aligned} \tag{43}$$

Besides, to compute $\mathscr{L}_{I_r}\left(\frac{\gamma r^{\alpha^{\mathrm{NL}}}}{PA^{\mathrm{NL}}}\right)$ for UAS 1 in the range of $r > d_1$, we propose Lemma 5.

Lemma 5. *$\mathscr{L}_{I_r}\left(\frac{\gamma r^{\alpha^{\mathrm{NL}}}}{PA^{\mathrm{NL}}}\right)$ for UAS 1 in the range of $r > d_1$ can be calculated by*

$$\mathscr{L}_{I_r}\left(\frac{\gamma r^{\alpha^{\mathrm{NL}}}}{PA^{\mathrm{NL}}}\right) = \exp\left(-2\pi\lambda\rho_2\left(\alpha^{\mathrm{NL}}, 1, \left(\gamma r^{\alpha^{\mathrm{NL}}}\right)^{-1}, r\right)\right), \quad (r > d_1), \tag{44}$$

where $\rho_2(\alpha, \beta, t, d)$ is defined in (30).

Proof: See Appendix E. ∎

To sum up, for UAS 1, T_2^{NL} can be evaluated as

$$T_2^{\mathrm{NL}} = \int_{d_1}^{\infty} \exp\left(-\frac{\gamma r^{\alpha^{\mathrm{NL}}} N_0}{PA^{\mathrm{NL}}}\right) \mathscr{L}_{I_r}\left(\frac{\gamma r^{\alpha^{\mathrm{NL}}}}{PA^{\mathrm{NL}}}\right) f_{R,2}^{\mathrm{NL}}(r)\, dr. \tag{45}$$

where $f_{R,2}^{\mathrm{NL}}(r)$ and $\mathscr{L}_{I_r}\left(\frac{\gamma r^{\alpha^{\mathrm{NL}}}}{PA^{\mathrm{NL}}}\right)$ are computed by (43) and (44), respectively.

5) The Result of $p^{cov}(\lambda,\gamma)$ and $A^{ASE}(\lambda,\gamma_0)$: Considering (25) and (41), $p^{\text{cov}}(\lambda,\gamma)$ for UAS 1 in 3GPP Case 1 can be written as

$$p^{\text{cov}}(\lambda,\gamma) = T_1^{\text{L}} + T_1^{\text{NL}} + T_2^{\text{NL}}, \tag{46}$$

where T_1^{L}, T_1^{NL} and T_2^{NL} are computed from closed-form expressions using (31), (38) and (45), respectively.

Plugging $p^{\text{cov}}(\lambda,\gamma)$ obtained from (46) into (10), we can get the result of $A^{\text{ASE}}(\lambda,\gamma_0)$ from (9) for UAS 1 in 3GPP case 1.

B. Analysis for UAS 2 in 3GPP Case 1

According to Theorem 2, $p^{\text{cov}}(\lambda,\gamma)$ for UAS 2 can then be obtained as

$$p^{\text{cov}}(\lambda,\gamma) = \sum_{n=1}^{2}\left(T_n^{\text{L}} + T_n^{\text{NL}}\right). \tag{47}$$

In the following sections, we investigate T_1^{L}, T_1^{NL}, T_2^{L}, and T_2^{NL}, respectively.

1) The Computation of T_1^L: From Theorem 2 and (47), and similar to (31), T_1^{L} can be derived as

$$T_1^{\text{L}} = \int_0^{d_1} \exp\left(-\frac{\gamma r^{\alpha^{\text{L}}} N_0}{PA^{\text{L}}}\right) \mathscr{L}_{I_r}\left(\frac{\gamma r^{\alpha^{\text{L}}}}{PA^{\text{L}}}\right) f_{R,1}^{\text{L}}(r)\, dr, \tag{48}$$

where according to Theorem 2 and (24), $f_{R,1}^{\text{L}}(r)$ is computed by

$$f_{R,1}^{\text{L}}(r) = \left(1-\frac{r}{d_1}\right) \times \exp\left(-\pi r^2\lambda\right) \times 2\pi r\lambda, \quad (0<r\le d_1). \tag{49}$$

To compute $\mathscr{L}_{I_r}\left(\frac{\gamma r^{\alpha^{\text{L}}}}{PA^{\text{L}}}\right)$ for UAS 2 in the range of $0<r\le d_1$, we propose Lemma 6.

Lemma 6. *$\mathscr{L}_{I_r}\left(\frac{\gamma r^{\alpha^{\text{L}}}}{PA^{\text{L}}}\right)$ for UAS 2 in the range of $0<r\le d_1$ can be calculated by*
$\mathscr{L}_{I_r}\left(\frac{\gamma r^{\alpha^{\text{L}}}}{PA^{\text{L}}}\right) =$

$$\begin{aligned}
&\exp\left(-2\pi\lambda\left(\rho_1\left(\alpha^{\text{L}},1,\left(\gamma r^{\alpha^{\text{L}}}\right)^{-1},d_1\right)-\rho_1\left(\alpha^{\text{L}},1,\left(\gamma r^{\alpha^{\text{L}}}\right)^{-1},r\right)\right)\right)\\
&\times\exp\left(\frac{2\pi\lambda}{d_0}\left(\rho_1\left(\alpha^{\text{L}},2,\left(\gamma r^{\alpha^{\text{L}}}\right)^{-1},d_1\right)-\rho_1\left(\alpha^{\text{L}},2,\left(\gamma r^{\alpha^{\text{L}}}\right)^{-1},r\right)\right)\right)\\
&\times\exp\left(-\frac{2\pi\lambda}{d_0}\left(\rho_1\left(\alpha^{\text{NL}},2,\left(\frac{\gamma A^{\text{NL}}}{A^{\text{L}}}r^{\alpha^{\text{L}}}\right)^{-1},d_1\right)-\rho_1\left(\alpha^{\text{NL}},2,\left(\frac{\gamma A^{\text{NL}}}{A^{\text{L}}}r^{\alpha^{\text{L}}}\right)^{-1},r\right)\right)\right)\\
&\times\exp\left(-2\pi\lambda\rho_2\left(\alpha^{\text{NL}},1,\left(\frac{\gamma A^{\text{NL}}}{A^{\text{L}}}r^{\alpha^{\text{L}}}\right)^{-1},d_1\right)\right), \quad (0<r\le d_1),
\end{aligned} \tag{50}$$

where $\rho_1(\alpha,\beta,t,d)$ and $\rho_2(\alpha,\beta,t,d)$ are defined in (29) and (30), respectively.

Proof: The proof is the same as the one provided in Appendix C with the substitution of r_1 with r, because in UAS 2 interference only comes from a distance larger than r. ■

2) The Computation of T_1^{NL}: From Theorem 2 and similar to (38), T_1^{NL} can be derived as

$$T_1^{\mathrm{NL}} = \int_0^{d_1} \exp\left(-\frac{\gamma r^{\alpha^{\mathrm{NL}}} N_0}{PA^{\mathrm{NL}}}\right) \mathscr{L}_{I_r}\left(\frac{\gamma r^{\alpha^{\mathrm{NL}}}}{PA^{\mathrm{NL}}}\right) f_{R,1}^{\mathrm{NL}}(r)\, dr, \tag{51}$$

where according to Theorem 2 and (24), $f_{R,1}^{\mathrm{NL}}(r)$ is computed by

$$f_{R,1}^{\mathrm{NL}}(r) = \frac{r}{d_1} \times \exp\left(-\pi r^2 \lambda\right) \times 2\pi r\lambda, \quad (0 < r \leq d_1). \tag{52}$$

To compute $\mathscr{L}_{I_r}\left(\frac{\gamma r^{\alpha^{\mathrm{NL}}}}{PA^{\mathrm{NL}}}\right)$ for UAS 2 in the range of $0 < r \leq d_1$, we propose Lemma 7.

Lemma 7. *$\mathscr{L}_{I_r}\left(\frac{\gamma r^{\alpha^{\mathrm{NL}}}}{PA^{\mathrm{NL}}}\right)$ for UAS 2 in the range of $0 < r \leq d_1$ can be calculated by* $\mathscr{L}_{I_r}\left(\frac{\gamma r^{\alpha^{\mathrm{NL}}}}{PA^{\mathrm{NL}}}\right) =$

$$\begin{aligned}
&\exp\left(-2\pi\lambda\left(\rho_1\left(\alpha^{\mathrm{L}}, 1, \left(\frac{\gamma A^{\mathrm{L}}}{A^{\mathrm{NL}}} r^{\alpha^{\mathrm{NL}}}\right)^{-1}, d_1\right) - \rho_1\left(\alpha^{\mathrm{L}}, 1, \left(\frac{\gamma A^{\mathrm{L}}}{A^{\mathrm{NL}}} r^{\alpha^{\mathrm{NL}}}\right)^{-1}, r\right)\right)\right) \\
&\times \exp\left(\frac{2\pi\lambda}{d_0}\left(\rho_1\left(\alpha^{\mathrm{L}}, 2, \left(\frac{\gamma A^{\mathrm{L}}}{A^{\mathrm{NL}}} r^{\alpha^{\mathrm{NL}}}\right)^{-1}, d_1\right) - \rho_1\left(\alpha^{\mathrm{L}}, 2, \left(\frac{\gamma A^{\mathrm{L}}}{A^{\mathrm{NL}}} r^{\alpha^{\mathrm{NL}}}\right)^{-1}, r\right)\right)\right) \\
&\times \exp\left(-\frac{2\pi\lambda}{d_0}\left(\rho_1\left(\alpha^{\mathrm{NL}}, 2, \left(\gamma r^{\alpha^{\mathrm{NL}}}\right)^{-1}, d_1\right) - \rho_1\left(\alpha^{\mathrm{NL}}, 2, \left(\gamma r^{\alpha^{\mathrm{NL}}}\right)^{-1}, r\right)\right)\right) \\
&\times \exp\left(-2\pi\lambda\rho_2\left(\alpha^{\mathrm{NL}}, 1, \left(\gamma r^{\alpha^{\mathrm{NL}}}\right)^{-1}, d_1\right)\right), \quad (0 < r \leq d_1),
\end{aligned} \tag{53}$$

where $\rho_1(\alpha, \beta, t, d)$ and $\rho_2(\alpha, \beta, t, d)$ are defined in (29) and (30), respectively.

Proof: The proof is the same as the one provided in Appendix D with the substitution of r_2 with r, because in UAS 2 interference only comes from a distance larger than r. ■

3) The Computation of T_2^{L}: From Theorem 2, (47), and similar to (39), T_2^{L} can be derived as

$$\begin{aligned}
T_2^{\mathrm{L}} &= \int_{d_1}^{\infty} \exp\left(-\frac{\gamma N_0}{P\zeta_2^{\mathrm{L}}(r)}\right) \mathscr{L}_{I_r}\left(\frac{\gamma}{P\zeta_2^{\mathrm{L}}(r)}\right) f_{R,2}^{\mathrm{L}}(r)\, dr \\
&= 0.
\end{aligned} \tag{54}$$

Note that the reason why $T_2^{\mathrm{L}} = 0$ in (54) is because according to Theorem 2 and (24), we have

$$\begin{aligned}
f_{R,2}^{\mathrm{L}}(r) &= 0 \times \exp\left(-\pi r^2 \lambda\right) \times 2\pi r\lambda \\
&= 0, \quad (r > d_1).
\end{aligned} \tag{55}$$

4) The Computation of T_2^{NL}: From Theorem 2 and similar to (45), T_2^{NL} can be derived as

$$T_2^{\mathrm{NL}} = \int_{d_1}^{\infty} \exp\left(-\frac{\gamma r^{\alpha^{\mathrm{NL}}} N_0}{P A^{\mathrm{NL}}}\right) \mathscr{L}_{I_r}\left(\frac{\gamma r^{\alpha^{\mathrm{NL}}}}{P A^{\mathrm{NL}}}\right) f_{R,2}^{\mathrm{NL}}(r)\, dr, \tag{56}$$

where according to Theorem 2 and (24), $f_{R,2}^{\mathrm{NL}}(r)$ is computed by

$$\begin{aligned} f_{R,2}^{\mathrm{NL}}(r) &= 1 \times \exp\left(-\pi r^2 \lambda\right) \times 2\pi r\lambda \\ &= \exp\left(-\pi\lambda r^2\right) \times 2\pi r\lambda, \quad (r > d_1). \end{aligned} \tag{57}$$

To compute $\mathscr{L}_{I_r}\left(\frac{\gamma r^{\alpha^{\mathrm{NL}}}}{P A^{\mathrm{NL}}}\right)$ for UAS 2 in the range of $r > d_1$, Lemma 5 is reused.

5) The Result of $p^{cov}(\lambda,\gamma)$ and $A^{ASE}(\lambda,\gamma_0)$: Considering (47) and (54), $p^{\mathrm{cov}}(\lambda,\gamma)$ for UAS 2 in 3GPP Case 1 can be written as

$$p^{\mathrm{cov}}(\lambda,\gamma) = T_1^{\mathrm{L}} + T_1^{\mathrm{NL}} + T_2^{\mathrm{NL}}, \tag{58}$$

where T_1^{L}, T_1^{NL} and T_2^{NL} are computed from closed-form expressions using (48), (51) and (56), respectively.

Plugging $p^{\mathrm{cov}}(\lambda,\gamma)$ obtained from (58) into (10), we can get the result of $A^{\mathrm{ASE}}(\lambda,\gamma_0)$ from (9) for UAS 2 in 3GPP case 1.

VI. Simulation and Discussion

In this Section, we use simulations to further study the performance of SCNs and establish the accuracy of our analysis. According to [13] and [14], we use the following parameters: $d_1 = 300$ m, $\alpha^{\mathrm{L}} = 2.09$, $\alpha^{\mathrm{NL}} = 3.75$, $A^{\mathrm{L}} = 10^{-4.11}$, $A^{\mathrm{NL}} = 10^{-3.29}$, $P = 24$ dBm, $N_0 = -95$ dBm (including a noise figure of 9 dB at the UE). Moreover, we study another 3GPP special case with an alternative LoS probability function, $\mathrm{Pr}^{\mathrm{L}}(r)$, using numerical integration to show the generality of our conclusions on the performance impact of LoS and NLoS transmissions.

A. Validation and Discussion of the Analytical Results of $p^{cov}(\lambda,\gamma)$

For 3GPP case 1 studied in Section V, and for both UASs, the results of $p^{\mathrm{cov}}(\lambda,\gamma)$ with $\gamma = 1$ and $\gamma = 10$ are plotted in Fig. 3 and Fig. 4, respectively. As can be observed from both figures, our analytical results perfectly match the simulation results. Since the results of $A^{\mathrm{ASE}}(\lambda,\gamma_0)$ are computed based on $p^{\mathrm{cov}}(\lambda,\gamma)$, we will only use analytical results on $p^{\mathrm{cov}}(\lambda,\gamma)$ in our discussion hereafter. For comparison, we have also included analytical results assuming a simplistic path loss model that does not differentiate LoS and NLoS transmissions [4]. Note that in [4], only one path loss exponent is defined and denoted by α. In our figures, α is set to α^{L} or α^{NL} respectively to show the results of the analysis from [4].

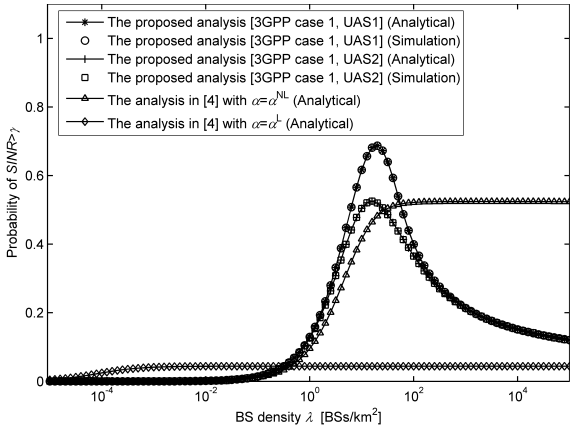

Fig. 3. $p^{\mathrm{cov}}(\lambda, 1)$ vs λ for 3GPP case 1.

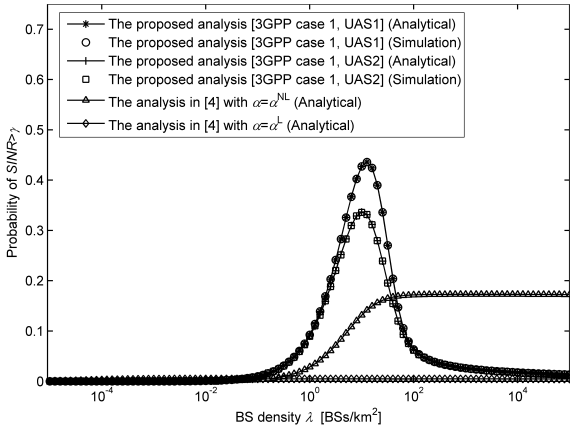

Fig. 4. $p^{\mathrm{cov}}(\lambda, 10)$ vs λ for 3GPP case 1.

From Fig. 3 and Fig. 4, we can observe that the coverage probability performance given by the stochastic geometry analysis in [4] first increases with the BS density because more BSs provide better coverage in noise-limited networks. Then, when λ is large enough, the coverage probability becomes independent of λ since the network is pushed into the interference-limited region, e.g., $\lambda > 10^{-1}$ BSs/km^2 and $\lambda > 10^2$ BSs/km^2 for the analysis from [4] with $\alpha = \alpha^{\mathrm{L}}$ and $\alpha = \alpha^{\mathrm{NL}}$, respectively. This observation is consistent with the conclusion in [4], which shows that for a sufficiently large λ, the coverage probability becomes almost a constant with the increase of the small cell density. The intuition behind the observation is that with the simplistic assumption on the path loss model, the increase in interference power is counterbalanced by the increase in signal power in a interference-limited network, and thus the coverage probability remains the same as λ further increases. Besides, we can find that the coverage probability performance of the analysis from [4] with $\alpha = \alpha^{\mathrm{NL}}$ is much better than that with $\alpha = \alpha^{\mathrm{L}}$ when λ is relatively large, e.g., $\lambda > 10\,\mathrm{BSs/km}^2$. The reason is that a larger path loss exponent allows a faster decay of the aggregated interference power, which has a dominating impact on the SINR performance for the UE, and hence the coverage probability performance improves as the path loss exponent α increases. The implication is that high path loss exponents help to separate adjacent small cells in the sense of less power leakage.

In Fig. 3 and Fig. 4, the coverage probability performance of the proposed stochastic geometry analysis for the 3GPP case 1 incorporating both LoS and NLoS transmissions exhibits a significant deviation from that of the analysis from [4], because when the distance r decreases, or equivalently when the small cell density λ increases, LoS transmission occurs with an increasingly higher probability than NLoS transmission. When the SCN is sparse and thus noise-limited, e.g., $\lambda \leq 10\,\mathrm{BSs/km}^2$, the coverage probability given by the proposed analysis grows as λ increases for the same reason as explained in the above paragraph, i.e., deploying more small cells is beneficial for removing coverage

holes. Then, when the network is dense enough and all coverage holes are removed, the coverage probability given by the proposed analysis decreases as λ increases, due to the transition of a large number of interference paths from NLoS to LoS. It is important to note that the coverage probability performance of the proposed analysis for 3GPP case 1 peaks at a certain value λ_0. Specifically, as λ increases above λ_0, interfering BSs may also be close to the typical UE and hence their signals may reach the UE via strong LoS paths too. Such crucial point can be readily obtained by setting the partial derivative of $p^{\text{cov}}(\lambda, \gamma)$ with regard to λ to zero, i.e., $\lambda_0 = \arg\limits_{\lambda} \left\{ \frac{\partial p^{\text{cov}}(\lambda,\gamma)}{\partial \lambda} = 0 \right\}$. The solution to this equation can be numerically found using a standard bisection searching [17]. In Fig. 3, the numerical results for λ_0 are 19.95 and 15.85 for UAS 1 and UAS 2, respectively. In comparison, in Fig. 4, the numerical results for λ_0 are 12.59 and 10.21 for UAS 1 and UAS 2, respectively.

It is also important to note that the proposed analysis incorporating both LoS and NLoS transmissions exhibits better coverage probability performance than the analysis from [4] with $\alpha = \alpha^{\text{NL}}$ when λ is relative small, e.g., $\lambda \leq 10\,\text{BSs/km}^2$. This is because with the proposed path loss model of (3) and the considered UASs, the signal is more likely to transmit via an LoS path while the interference from interfering BSs further away is more likely to suffer more attenuation due to NLoS paths caused by more obstacles along the longer distance. Moreover, the performance of UAS 1 is strictly superior to that of UAS 2 because the UE is always associate with the BS with the smallest path loss in UAS 1, leading to a better coverage performance. However, such performance superiority is noticeable only when $1 \leq \lambda \leq 10^2\,\text{BSs/km}^2$, where the transition of interference paths from NLoS to LoS frequently take place. When λ is tremendously large, e.g., $\lambda \geq 10^4\,\text{BSs/km}^2$, the coverage probability decreases at a very slow pace because both the signal power and the interference power are LoS dominated and thus statistically stable.

To sum up, our results are in stark contrast with those of the analysis in [4] assuming a simplistic path loss model that does not differentiate LoS and NLoS transmissions. The implication is profound. Particularly, the conventional stochastic geometry analysis leads to the conclusion that the cell splitting gain resulting from spectrum reuse can be surely achieved in dense SCNs since the coverage probability is invariant with λ. In contrast, our theoretical analysis shows that the coverage probability will initially increase with the increase of λ, but when λ is larger than λ_0, the coverage probability will decrease as small cells become denser in practical SCNs, where the decrease is caused by the transition of a large number of interference paths from NLoS to LoS. Considering such trend of the coverage probability and looking at the ASE expression in (9), we can conclude that the trend of the ASE performance for SCNs should be complicated and it will be investigated in the next subsection.

B. Discussion of the Analytical Results of $A^{ASE}(\lambda, \gamma_0)$

In this subsection, we first investigate the analytical results of $A^{\mathrm{ASE}}(\lambda, \gamma_0)$ with $\gamma_0 = 1$, based on the analytical results of $p^{\mathrm{cov}}(\lambda, \gamma)$. The results of $A^{\mathrm{ASE}}(\lambda, 1)$ are plotted in Fig. 5, comparing the proposed stochastic geometry analysis with the analysis from [4] with $\alpha = \alpha^{\mathrm{L}}$ and $\alpha = \alpha^{\mathrm{NL}}$, respectively.

As can be seen from Fig. 5, the analysis from [4] indicates that when the SCN is dense enough, e.g., $\lambda \geq 10^2$ BSs/km^2, the ASE performance increases linearly with λ, which is logically correct from the conclusion that $p^{\mathrm{cov}}(\lambda, \gamma)$ is invariable with respect to λ for a given γ in dense SCNs [4]. In contrast, the proposed stochastic geometry analysis for the 3GPP case 1 reveals a more complicated trend for the ASE performance. Specifically, when the SCN is relatively sparse, e.g., $\lambda \leq \lambda_0$ BSs/km^2, the ASE quickly increases with λ because the network is generally noise-limited, thus adding more small cells immensely benefits the ASE. When the SCN is extremely dense, e.g., $\lambda \geq 10^4$ BSs/km^2, the ASE exhibits a nearly linear trajectory with regard to λ because both the signal power and the interference power are now LoS dominated and thus statistically stable as explained before. As for the practical range of λ, i.e., $\lambda \in [\lambda_0, 10^4]$ BSs/km^2, the ASE first exhibits a slowing-down in the rate of growth due to the fast decrease of the coverage probability at around $\lambda \in [\lambda_0, \lambda_1]$ BSs/km^2 as shown in Fig. 3, where λ_1 is another threshold larger than λ_0. When $\lambda \geq \lambda_1$, the ASE will pick up the growth rate as the decrease of the coverage probability becomes negligible. In Fig. 3, the value of λ_1 seems to be around 10^3 BSs/km^2.

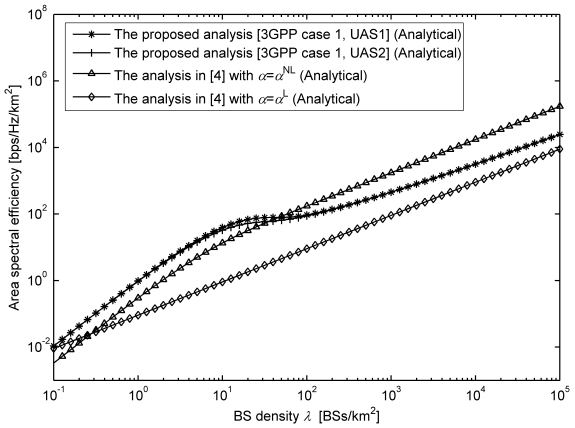

Fig. 5. $A^{\mathrm{ASE}}(\lambda, 1)$ vs λ for 3GPP case 1.

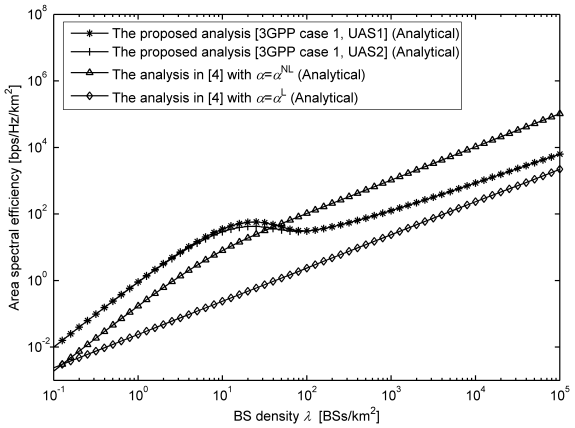

Fig. 6. $A^{\mathrm{ASE}}(\lambda, 10)$ vs λ for 3GPP case 1.

In the following, we investigate the impact of γ_0 on $A^{\mathrm{ASE}}(\lambda, \gamma_0)$ by showing the results of $A^{\mathrm{ASE}}(\lambda, 10)$ in Fig. 6. An interesting observation is that the ASE of the proposed stochastic geometry analysis even decreases with the increase of λ at around $[10, 10^2]$ BSs/km^2, indicating the significant impact of the path loss model incorporating both NLoS and LoS transmissions. Such impact makes

a difference for SCNs in terms of the ASE both quantitatively and qualitatively, compared with the SCNs with a simplistic path loss model that does not differentiate LoS and NLoS transmissions. As a confirmation, note that comparing Fig. 3 and Fig. 4, we can observe that increasing γ_0 from 1 to 10 will greatly accelerate the decrease of the coverage probability at around $\lambda \in \left[10, 10^2\right]$ BSs/km^2, which in turn causes the decrease of the ASE at that range of λ in Fig. 6.

To sum up, our theoretical analysis concludes that when the density of small cells is larger than λ_0, the ASE suffers from a slow growth or even a notable *decrease* as λ increases, because of the decrease of the network coverage probability, as discussed in Subsection VI-A. Furthermore, the ASE will grow almost linearly as the small cell density increases above λ_1.

With the thresholds λ_0 and λ_1, SCNs can be roughly classified into 3 categories, i.e., the sparse SCN ($0 < \lambda \leq \lambda_0$), the dense SCN ($\lambda_0 < \lambda \leq \lambda_1$) and the very dense SCN ($\lambda > \lambda_1$). The ASEs for both the sparse SCN and the very dense SCN grow almost linearly with the increase of λ, while the ASE of the dense SCN shows a slow growth or even a notable decrease with the increase of λ. From Fig. 5 and Fig. 6, we can get a new look at the ultra-dense SCN, which has been identified as one of the key enabling technologies of the 5th-generation (5G) networks [2]. Up to now, there is no clear view in both industry and academia on how dense a SCN can be categorized as an ultra-dense SCN. According to our study, for 3GPP case 1, we propose that the 5G systems should target the third kind of SCNs as ultra-dense SCNs, i.e., the SCNs with $\lambda > \lambda_1$, because the associated ASE will grow almost linearly as λ increases since both the signal power and the interference power are LoS dominated and thus statistically stable. Numerically speaking, λ_1 is around 10^3 BSs/km^2 in Fig. 5 and Fig. 6. It is important to note that the second category of SCNs ($\lambda_0 < \lambda \leq \lambda_1$) is better to be avoided in practical SCN deployments due to its cost-inefficiency.

C. Investigation of $A^{ASE}(\lambda, \gamma_0)$ for an Alternative $Pr^L(r)$

As another application of our analytical work and to demonstrate that the conclusions obtained on the performance impact of LoS and NLoS transmissions have general significance, we consider another widely used LoS probability function adopted by the 3GPP as [13]

$$\Pr^{\mathrm{L}}(r) = 0.5 - \min\left\{0.5, 5\exp\left(-\frac{R_1}{r}\right)\right\} + \min\left\{0.5, 5\exp\left(-\frac{r}{R_2}\right)\right\}, \tag{59}$$

where $R_1 = 156$ m and $R_2 = 30$ m. To show how $\Pr^{\mathrm{L}}(r)$ in (59) can be fitted into our general path loss model proposed in (3), we reformulate (59) as

$$\Pr^{\mathrm{L}}(r) = \begin{cases} 1-\frac{1}{2}\exp\left(-R_1/r\right), & 0 \le r \le d_1 \\ \frac{1}{2}\exp\left(-r/R_2\right), & r > d_1 \end{cases}, \tag{60}$$

where $d_1 = \frac{R_1}{\ln 10}$. The combination of the LoS probability function in (60) and the path loss formula in (23) can then be deemed as a special case of the proposed general path loss model addressed in (3) with the following substitution: $N = 2$, $\zeta_1^{\mathrm{L}}(r) = \zeta_2^{\mathrm{L}}(r) = A^{\mathrm{L}} r^{-\alpha^{\mathrm{L}}}$, $\zeta_1^{\mathrm{NL}}(r) = \zeta_2^{\mathrm{NL}}(r) = A^{\mathrm{NL}} r^{-\alpha^{\mathrm{NL}}}$, $\Pr_1^{\mathrm{L}}(r) = 1 - \frac{1}{2}\exp\left(-R_1/r\right)$, and $\Pr_2^{\mathrm{L}}(r) = \frac{1}{2}\exp\left(-r/R_2\right)$. For clarity, this 3GPP special case is referred to as 3GPP case 2 in the sequel.

Due to the complicated expressions of $\Pr^{\mathrm{L}}(r)$ in (60), closed-form expressions of $p^{\mathrm{cov}}(\lambda, \gamma)$ like those in (25) and (47) are difficult to obtain. Here, we evaluate the network performance for 3GPP case 2 by applying numerical integration on Theorem 1 and Theorem 2. The results of $p^{\mathrm{cov}}(\lambda, 1)$ and $A^{\mathrm{ASE}}(\lambda, 1)$ for 3GPP case 2 are plotted in Fig. 7 and Fig. 8, respectively. As can be seen from both figures, our analytical results are accurate compared with the simulation results and all the observations in Subsections VI-A and VI-B are qualitatively valid for Fig. 7 and Fig. 8 except for some quantitative deviation. Specifically, in Fig. 7, the numerical results for λ_0 are 98.72 and 79.43 for UAS 1 and UAS 2, respectively. In Fig. 8, the ASE is also shown to suffers from a slow growth or even a slight decrease as λ increases when $\lambda > \lambda_0$, because of the decrease of the network coverage probability shown in Fig. 7. Furthermore, the ASE will grow almost linearly as λ increases above another larger threshold λ_1. Such λ_1 is in the order of several 10^3 BSs/km^2 as shown in Fig. 8. Therefore as expected, changing the LoS probability function may only cause quantitative difference on the coverage probability and the ASE, but the trend observed on the network performance remains the same. Thus, the results obtained in this paper on the performance impact of LoS and NLoS transmissions have general significance and may not be affected by the particular path loss model being considered.

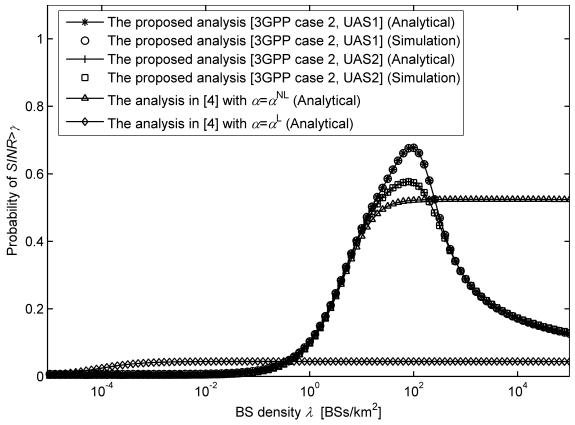

Fig. 7. $p^{\mathrm{cov}}(\lambda, 1)$ vs λ for 3GPP case 2.

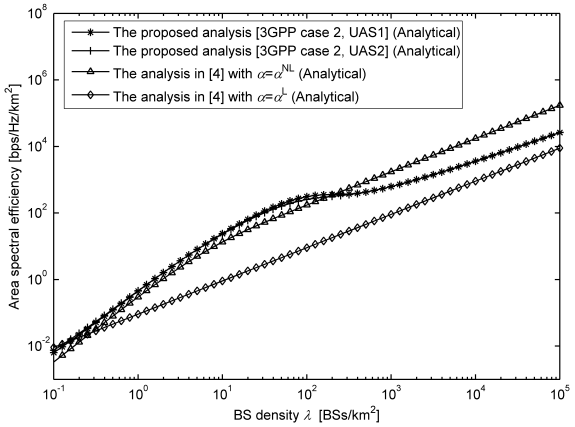

Fig. 8. $A^{\mathrm{ASE}}(\lambda, 1)$ vs λ for 3GPP case 2.

VII. Conclusion

In this paper, we show that a sophisticated path loss model incorporating both LoS and NLoS transmissions has a significant impact on the performance of SCNs, measured by the two metrics of the coverage probability and the ASE. Such impact is not only quantitative but also qualitative. Specifically, our theoretical analysis concludes that the network coverage probability will initially increase with the increase of the small cell density, but when the density of small cells is larger than a threshold λ_0, the network coverage probability will decrease as small cells become denser in practical SCNs, which in turn makes the ASE suffer from a slow growth or even a notable *decrease* as the small cell density increases. Furthermore, the ASE will grow almost linearly as the small cell density increases above another larger threshold λ_1. The intuition behind our conclusion is that when the density of small cells is larger than a threshold, the interference power will increase faster than the signal power due to the transition of a large number of interference paths from NLoS to LoS, and thus the small cell density matters!

For practical regime of small cell density, the performance results derived from our analysis are distinctively different from previous results considering a simplistic path loss model that does not differentiate LoS and NLoS transmissions. It is therefore important to consider a path loss model incorporating both LoS and NLoS transmission when studying the performance of dense SCNs. Specifically, previous results predict that the ASE should monotonically grows with the increase of the small cell density. However, our results show that the ASE will not necessarily improves with the increase of the small cell density, which sheds valuable insights on the design and deployment of future small cell.

Finally, according to our study, for 3GPP cases, we propose that the 5G systems should target the SCNs as ultra-dense SCNs with $\lambda > \lambda_1$, because the associated ASE will grow almost linearly as λ increases. Numerically speaking, λ_1 appears to be around several 10^3 BSs/km^2 from our results.

As our future work, we will consider other factors of realistic networks in the theoretical analysis of SCNs, such as practical directional antennas or sophisticated beam-forming functions. Another future work is the introduction of an even more sophisticated multi-path fading model into the analysis of SCNs because the multi-path fading model is also affected by LoS and NLoS transmissions.

Appendix A: Proof of Theorem 1

For clarity, we first summarize our basic ideas to prove Theorem 1. In order to evaluate $p^{\text{cov}}(\lambda, \gamma)$, the first key step is to calculate the PDFs of the events that the typical UE is associated with a BS

with an LoS path or an NLoS path, taking the proposed path loss model of (3) into account. The second key step is to calculate the probability of $\Pr\left[\mathrm{SINR}>\gamma\right]$ conditioned on distance r.

Logically, according to UAS 1, the event that the UE is associated with a BS with an LoS path at distance r is equivalent to the joint event that the UE is associated with a nearest LoS BS and there is no NLoS BS gives a smaller path loss than such nearest LoS BS. Similarly, according to UAS 1, the event that the UE is associated with a BS with an NLoS path at distance r is equivalent to the joint event that the UE is associated with a nearest NLoS BS and there is no LoS BS gives a smaller path loss than such nearest NLoS BS. Besides, the metric $\Pr\left[\mathrm{SINR}>\gamma\right]$ should be evaluated based on our assumption on the distribution of the multi-path fading RV, i.e., the exponential distribution. Following the summarized thoughts, we provide our proof of Theorem 1 in the sequel.

From (6) and (7), we can derive $p^{\mathrm{cov}}\left(\lambda,\gamma\right)$ in a straightforward way as

$$\begin{aligned}
p^{\mathrm{cov}}\left(\lambda,\gamma\right) &\overset{(a)}{=} \int_{r>0}\Pr\left[\mathrm{SINR}>\gamma|\,r\right]f_R\left(r\right)dr\\
&= \int_{r>0}\Pr\left[\frac{P\zeta\left(r\right)h}{I_r+N_0}>\gamma\middle|\,r\right]f_R\left(r\right)dr\\
&= \int_0^{d_1}\Pr\left[\frac{P\zeta_1^{\mathrm{L}}\left(r\right)h}{I_r+N_0}>\gamma\right]f_{R,1}^{\mathrm{L}}\left(r\right)dr+\int_0^{d_1}\Pr\left[\frac{P\zeta_1^{\mathrm{NL}}\left(r\right)h}{I_r+N_0}>\gamma\right]f_{R,1}^{\mathrm{NL}}\left(r\right)dr\\
&\quad+\cdots\\
&\quad+\int_{d_{N-1}}^{\infty}\Pr\left[\frac{P\zeta_N^{\mathrm{L}}\left(r\right)h}{I_r+N_0}>\gamma\right]f_{R,N}^{\mathrm{L}}\left(r\right)dr+\int_{d_{N-1}}^{\infty}\Pr\left[\frac{P\zeta_N^{\mathrm{NL}}\left(r\right)h}{I_r+N_0}>\gamma\right]f_{R,N}^{\mathrm{NL}}\left(r\right)dr\\
&\overset{\triangle}{=} \sum_{n=1}^{N}\left(T_n^{\mathrm{L}}+T_n^{\mathrm{NL}}\right),
\end{aligned}\tag{61}$$

where T_n^{L} and T_n^{NL} are piece-wise functions defined as $T_n^{\mathrm{L}}=\int_{d_{n-1}}^{d_n}\Pr\left[\frac{P\zeta_n^{\mathrm{L}}(r)h}{I_r+N_0}>\gamma\right]f_{R,n}^{\mathrm{L}}\left(r\right)dr$ and $T_n^{\mathrm{NL}}=\int_{d_{n-1}}^{d_n}\Pr\left[\frac{P\zeta_n^{\mathrm{NL}}(r)h}{I_r+N_0}>\gamma\right]f_{R,n}^{\mathrm{NL}}\left(r\right)dr$, respectively. Besides, d_0 and d_N are respectively defined as 0 and ∞. Moreover, $f_{R,n}^{\mathrm{L}}\left(r\right)$ and $f_{R,n}^{\mathrm{NL}}\left(r\right)$ are the piece-wise PDFs of the event that the UE is associated with a BS with an LoS path at distance r based on UAS 1 and the event that the UE is associated with a BS with an NLoS path at distance r based on UAS 1, respectively. All the $f_{R,n}^{\mathrm{L}}\left(r\right)$ and $f_{R,n}^{\mathrm{NL}}\left(r\right)$ are stacked into $f_R\left(r\right)$ in (a) of (61), and $f_R\left(r\right)$ is defined in a similar form as in (3):

$$f_R\left(r\right) = \begin{cases}
f_{R,1}\left(r\right)=\begin{cases}f_{R,1}^{\mathrm{L}}\left(r\right), & \text{the UE is associated with an LoS BS}\\ f_{R,1}^{\mathrm{NL}}\left(r\right), & \text{the UE is associated with an NLoS BS}\end{cases}, & 0\le r\le d_1\\
f_{R,2}\left(r\right)=\begin{cases}f_{R,2}^{\mathrm{L}}\left(r\right), & \text{the UE is associated with an LoS BS}\\ f_{R,2}^{\mathrm{NL}}\left(r\right), & \text{the UE is associated with an NLoS BS}\end{cases}, & d_1<r\le d_2\\
\vdots & \vdots\\
f_{R,N}\left(r\right)=\begin{cases}f_{R,N}^{\mathrm{L}}\left(r\right), & \text{the UE is associated with an LoS BS}\\ f_{R,N}^{\mathrm{NL}}\left(r\right), & \text{the UE is associated with an NLoS BS}\end{cases}, & r>d_{N-1}
\end{cases}\tag{62}$$

Regarding $f_{R,n}^{\mathrm{L}}(r)$ in (61), we define two events as follows, the joint event of which is equivalent to the event that the UE is associated with a BS with an LoS path at distance r according to UAS 1.

- Event B^{L}: the nearest BS with an LoS path is located at distance r
- Event $C^{N\mathrm{L}}$: there is no BS with an NLoS path in the disk centered on the UE with a radius of $r_1 < r$, where r_1 satisfies $\zeta_n^{\mathrm{L}}(r) = \zeta_n^{\mathrm{NL}}(r_1)$

Note that Event B^{L} guarantees that the path loss associated with *an arbitrary LoS BS* with a distance greater than r is always larger than that associated with *the considered LoS BS* at distance r. Besides, Event $C^{N\mathrm{L}}$guarantees that the path loss associated with *an arbitrary NLoS BS* with a distance greater than r_1 is always larger than that associated with *the considered LoS BS* at distance r.

According to [4], the cumulative density function (CDF) of Event B^{L} with regard to r is given by

$$F_{R,n}^{B^{\mathrm{L}}}(r) = 1 - \exp\left(-\int_0^r \Pr^{\mathrm{L}}(u)\, 2\pi u\lambda du\right), \quad (d_{n-1} < r \le d_n). \tag{63}$$

Hence, taking the derivative of $F_{R,n}^{B^{\mathrm{L}}}(r)$ with regard to r, yields the PDF of Event B^{L} as

$$f_{R,n}^{B^{\mathrm{L}}}(r) = \exp\left(-\int_0^r \Pr^{\mathrm{L}}(u)\, 2\pi u\lambda du\right) \times \Pr_n^{\mathrm{L}}(r) \times 2\pi r\lambda, \quad (d_{n-1} < r \le d_n). \tag{64}$$

The PDF $f_{R,n}^{B^{\mathrm{L}}}(r)$ should be further thinned by the probability of Event C^{NL} on condition of r, which is $\exp\left(-\int_0^{r_1}\left(1-\Pr^{\mathrm{L}}(u)\right)2\pi u\lambda du\right)$ [4], and we can get the PDF of the joint event of B^{L} and C^{NL}:

$$f_{R,n}^{\mathrm{L}}(r) = \exp\left(-\int_0^{r_1}\left(1-\Pr^{\mathrm{L}}(u)\right)2\pi u\lambda du\right) \times f_{R,n}^{B^{\mathrm{L}}}(r). \tag{65}$$

As for the calculation of $\Pr\left[\frac{P\zeta_n^{\mathrm{L}}(r)h}{I_r+N_0} > \gamma\right]$ in (61), we have

$$\begin{aligned}\Pr\left[\frac{P\zeta_n^{\mathrm{L}}(r)\,h}{I_r+N_0} > \gamma\right] &= \mathbb{E}_{[I_r]}\left\{\Pr\left[h > \frac{\gamma(I_r+N_0)}{P\zeta_n^{\mathrm{L}}(r)}\right]\right\} \\ &= \mathbb{E}_{[I_r]}\left\{\bar{F}_H\left(\frac{\gamma(I_r+N_0)}{P\zeta_n^{\mathrm{L}}(r)}\right)\right\},\end{aligned} \tag{66}$$

where $\mathbb{E}_{[X]}\{\cdot\}$ denotes the expectation operation taking the expectation over the variable X and $\bar{F}_H(h)$ denotes the complementary cumulative density function (CCDF) of RV h. Since we assume h to be an exponential RV, we have $\bar{F}_H(h) = \exp(-h)$ and thus (66) can be further derived as

$$\begin{aligned}\Pr\left[\frac{P\zeta_n^{\mathrm{L}}(r)\,h}{I_r+N_0} > \gamma\right] &= \mathbb{E}_{[I_r]}\left\{\exp\left(-\frac{\gamma(I_r+N_0)}{P\zeta_n^{\mathrm{L}}(r)}\right)\right\} \\ &= \exp\left(-\frac{\gamma N_0}{P\zeta_n^{\mathrm{L}}(r)}\right)\mathbb{E}_{[I_r]}\left\{\exp\left(-\frac{\gamma}{P\zeta_n^{\mathrm{L}}(r)}I_r\right)\right\} \\ &= \exp\left(-\frac{\gamma N_0}{P\zeta_n^{\mathrm{L}}(r)}\right)\mathscr{L}_{I_r}\left(\frac{\gamma}{P\zeta_n^{\mathrm{L}}(r)}\right),\end{aligned} \tag{67}$$

where $\mathscr{L}_{I_r}(s)$ is the Laplace transform of RV I_r evaluated at s.

Regarding $f_{R,n}^{\mathrm{NL}}(r)$ in (61), we also define two events, the joint event of which is equivalent to the event that the UE is associated with a BS with an NLoS path at distance r according to UAS 1.

- Event B^{NL}: the nearest BS with an NLoS path is located at distance r
- Event C^{L}: there is no BS with an LoS path in the disk centered on the UE with a radius of r_2, where r_2 satisfies $\zeta_n^{\mathrm{L}}(r_2) = \zeta_n^{\mathrm{NL}}(r)$

Note that Event B^{NL} guarantees that the path loss associated with *an arbitrary NLoS BS* with a distance greater than r is always larger than that associated with *the considered NLoS BS* at distance r. Besides, Event C^{NL}guarantees that the path loss associated with *an arbitrary LoS BS* with a distance greater than r_2 is always larger than that associated with *the considered NLoS BS* at r.

According to [4], the CDF of Event B^{NL} with regard to r is written as

$$F_{R,n}^{B^{\mathrm{NL}}}(r) = 1-\exp\left(-\int_0^r \left(1-\Pr^{\mathrm{L}}(u)\right)2\pi u\lambda du\right), \quad (d_{n-1}<r\le d_n). \tag{68}$$

Hence, taking the derivative of $F_{R,n}^{B^{\mathrm{NL}}}(r)$ with regard to r, yields the PDF of Event B^{NL} as

$$f_{R,n}^{B^{\mathrm{NL}}}(r) = \exp\left(-\int_0^r \left(1-\Pr^{\mathrm{L}}(u)\right)2\pi u\lambda du\right)\times\left(1-\Pr_n^{\mathrm{L}}(r)\right)2\pi r\lambda, \quad (d_{n-1}<r\le d_n) \tag{69}$$

Similar to (65), the PDF $f_{R,n}^{B^{\mathrm{NL}}}(r)$ should be further thinned by the probability of Event C^{L} on condition of r, which is $\exp\left(-\int_0^{r_2}\Pr^{\mathrm{L}}(u)\,2\pi u\lambda du\right)$ [4], so that we can get the PDF of the joint event of B^{NL} and C^{L} as

$$f_{R,n}^{\mathrm{NL}}(r) = \exp\left(-\int_0^{r_2}\Pr^{\mathrm{L}}(u)\,2\pi u\lambda du\right)\times f_{R,n}^{B^{\mathrm{NL}}}(r). \tag{70}$$

As for the calculation of $\Pr\left[\frac{P\zeta_n^{\mathrm{NL}}(r)h}{I_r+N_0}>\gamma\right]$ in (61), we have

$$\begin{aligned}\Pr\left[\frac{P\zeta_n^{\mathrm{NL}}(r)\,h}{I_r+N_0}>\gamma\right] &= \mathbb{E}_{[I_r]}\left\{\Pr\left[h>\frac{\gamma\left(I_r+N_0\right)}{P\zeta_n^{\mathrm{NL}}(r)}\right]\right\}\\ &= \mathbb{E}_{[I_r]}\left\{\bar{F}_H\left(\frac{\gamma\left(I_r+N_0\right)}{P\zeta_n^{\mathrm{NL}}(r)}\right)\right\}.\end{aligned} \tag{71}$$

Since $\bar{F}_H(h)=\exp(-h)$, thus (71) can be further derived as

$$\begin{aligned}\Pr\left[\frac{P\zeta_n^{\mathrm{NL}}(r)\,h}{I_r+N_0}>\gamma\right] &= \mathbb{E}_{[I_r]}\left\{\exp\left(-\frac{\gamma\left(I_r+N_0\right)}{P\zeta_n^{\mathrm{NL}}(r)}\right)\right\}\\ &= \exp\left(-\frac{\gamma N_0}{P\zeta_n^{\mathrm{NL}}(r)}\right)\mathbb{E}_{[I_r]}\left\{\exp\left(-\frac{\gamma}{P\zeta_n^{\mathrm{NL}}(r)}I_r\right)\right\}\\ &= \exp\left(-\frac{\gamma N_0}{P\zeta_n^{\mathrm{NL}}(r)}\right)\mathscr{L}_{I_r}\left(\frac{\gamma}{P\zeta_n^{\mathrm{NL}}(r)}\right).\end{aligned} \tag{72}$$

Our proof of Theorem 1 is completed by plugging (65), (67), (70) and (72) into (61).

APPENDIX B: PROOF OF THEOREM 2

The proof of Theorem 2 is very similar to that of Theorem 1. First, from (6) and (7), we can reuse (61) as the general result of $p^{\text{cov}}(\lambda,\gamma)$ for UAS 2. However, $f^{\text{L}}_{R,n}(r)$ and $f^{\text{NL}}_{R,n}(r)$ should be specifically derived for UAS 2 as follows.

Regarding $f^{\text{L}}_{R,n}(r)$, we define two events as follows, the joint event of which is equivalent to the event that the UE is associated with a BS with an LoS path at distance r based on UAS 2.

- Event B: the nearest BS is located at distance r
- Event D^{L}: the BS is one with an LoS path

According to [4], the cumulative density function (CDF) of Event B with regard to r is given by

$$F^{B}_{R,n}(r) \;=\; 1-\exp\left(-\pi r^2\lambda\right), \quad (d_{n-1}<r\leq d_n). \tag{73}$$

Hence, taking the derivative of $F^{B}_{R,n}(r)$ with regard to r, yields the PDF of Event B as

$$f^{B}_{R,n}(r) \;=\; \exp\left(-\pi r^2\lambda\right)\times 2\pi r\lambda, \quad (d_{n-1}<r\leq d_n). \tag{74}$$

The PDF $f^{B}_{R,n}(r)$ should be further thinned by the probability of Event D^{L} on condition of r, which is $\Pr^{\text{L}}_{n}(r)$, so that we can get the PDF of the joint event of B and C^{NL} as

$$f^{\text{L}}_{R,n}(r) \;=\; \Pr^{\text{L}}_{n}(r)\times f^{B}_{R,n}(r). \tag{75}$$

Regarding $f^{\text{NL}}_{R,n}(r)$, we also define two events as follows, the joint event of which is equivalent to the event that the UE is associated with a BS with an NLoS path at distance r based on UAS 1.

- Event B: the nearest BS is located at distance r
- Event D^{NL}: the BS is one with an NLoS path

Similar to (75), the PDF $f^{B}_{R,n}(r)$ should be further thinned by the probability of Event D^{L} on condition of r, which is $\left(1-\Pr^{\text{L}}_{n}(r)\right)$, so that we can get the PDF of the joint event of B and D^{L} as

$$f^{\text{NL}}_{R,n}(r) \;=\; \left(1-\Pr^{\text{L}}_{n}(r)\right)\times\exp\left(-\pi r^2\lambda\right)\times 2\pi r\lambda, \quad (d_{n-1}<r\leq d_n). \tag{76}$$

Our proof of Theorem 2 is completed by plugging (75), (67), (76) and (72) into (61).

APPENDIX C: PROOF OF LEMMA 3

Based on the assumption of UAS 1, it is straightforward to derive $\mathscr{L}_{I_r}(s)$ in the range of $0<r\leq d_1$ as

$$\begin{aligned}
\mathscr{L}_{I_r}(s) &= \mathbb{E}_{[I_r]}\left\{\exp\left(-sI_r\right)\middle|\, 0<r\le d_1\right\} \\
&= \mathbb{E}_{[\Phi,\{\beta_i\},\{g_i\}]}\left\{\exp\left(-s\sum_{i\in\Phi/b_o} P\beta_i g_i\right)\middle|\, 0<r\le d_1\right\} \\
&= \mathbb{E}_{[\Phi]}\left\{\prod_{i\in\Phi/b_o}\mathbb{E}_{[\beta,g]}\left\{\exp\left(-sP\beta g\right)\right\}\middle|\, 0<r\le d_1\right\} \\
&\overset{(a)}{=} \exp\left(-2\pi\lambda\int_r^{\infty}\left(1-\mathbb{E}_{[g]}\left\{\exp\left(-sP\beta\left(u\right)g\right)\right\}\right)udu\middle|\, 0<r\le d_1\right), \qquad (77)
\end{aligned}$$

where (a) in (77) is obtained from [4].

Since $0<r\le d_1$, $\mathbb{E}_{[g]}\left\{\exp\left(-sP\beta\left(u\right)g\right)\right\}$ in (77) should consider interference from both LoS and NLoS paths. Thus, $\mathscr{L}_{I_r}(s)$ can be further derived as

$$\begin{aligned}
\mathscr{L}_{I_r}(s) &= \exp\left(-2\pi\lambda\int_r^{d_1}\left(1-\frac{u}{d_1}\right)\left[1-\mathbb{E}_{[g]}\left\{\exp\left(-sPA^{\mathrm{L}}u^{-\alpha^{\mathrm{L}}}g\right)\right\}\right]udu\right) \\
&\quad\times\exp\left(-2\pi\lambda\int_{r_1}^{d_1}\frac{u}{d_1}\left[1-\mathbb{E}_{[g]}\left\{\exp\left(-sPA^{\mathrm{NL}}u^{-\alpha^{\mathrm{NL}}}g\right)\right\}\right]udu\right) \\
&\quad\times\exp\left(-2\pi\lambda\int_{d_1}^{\infty}\left[1-\mathbb{E}_{[g]}\left\{\exp\left(-sPA^{\mathrm{NL}}u^{-\alpha^{\mathrm{NL}}}g\right)\right\}\right]udu\right) \\
&= \exp\left(-2\pi\lambda\int_r^{d_1}\left(1-\frac{u}{d_1}\right)\frac{u}{1+\left(sPA^{\mathrm{L}}\right)^{-1}u^{\alpha^{\mathrm{L}}}}du\right) \\
&\quad\times\exp\left(-2\pi\lambda\int_{r_1}^{d_1}\frac{u}{d_1}\frac{u}{1+\left(sPA^{\mathrm{NL}}\right)^{-1}u^{\alpha^{\mathrm{NL}}}}du\right) \\
&\quad\times\exp\left(-2\pi\lambda\int_{d_1}^{\infty}\frac{u}{1+\left(sPA^{\mathrm{NL}}\right)^{-1}u^{\alpha^{\mathrm{NL}}}}du\right). \qquad (78)
\end{aligned}$$

Based on (78), $\mathscr{L}_{I_r}\left(\frac{\gamma r^{\alpha^{\mathrm{L}}}}{PA^{\mathrm{L}}}\right)$ for UAS 1 in the range of $0<r\le d_1$ can be further written as $\mathscr{L}_{I_r}\left(\frac{\gamma r^{\alpha^{\mathrm{L}}}}{PA^{\mathrm{L}}}\right)=$

$$\begin{aligned}
&\exp\left(-2\pi\lambda\left(\int_0^{d_1}\frac{u}{1+\left(\gamma r^{\alpha^{\mathrm{L}}}\right)^{-1}u^{\alpha^{\mathrm{L}}}}du-\int_0^{r}\frac{u}{1+\left(\gamma r^{\alpha^{\mathrm{L}}}\right)^{-1}u^{\alpha^{\mathrm{L}}}}du\right)\right) \\
&\times\exp\left(-2\pi\lambda\frac{-1}{d_1}\left(\int_0^{d_1}\frac{u^2}{1+\left(\gamma r^{\alpha^{\mathrm{L}}}\right)^{-1}u^{\alpha^{\mathrm{L}}}}du-\int_0^{r}\frac{u^2}{1+\left(\gamma r^{\alpha^{\mathrm{L}}}\right)^{-1}u^{\alpha^{\mathrm{L}}}}du\right)\right) \\
&\times\exp\left(-2\pi\lambda\frac{1}{d_1}\left(\int_0^{d_1}\frac{u^2}{1+\left(\frac{\gamma A^{\mathrm{NL}}}{A^{\mathrm{L}}}r^{\alpha^{\mathrm{L}}}\right)^{-1}u^{\alpha^{\mathrm{NL}}}}du-\int_0^{r_1}\frac{u^2}{1+\left(\frac{\gamma A^{\mathrm{NL}}}{A^{\mathrm{L}}}r^{\alpha^{\mathrm{L}}}\right)^{-1}u^{\alpha^{\mathrm{NL}}}}du\right)\right) \\
&\times\exp\left(-2\pi\lambda\int_{d_1}^{\infty}\frac{u}{1+\left(\frac{\gamma A^{\mathrm{NL}}}{A^{\mathrm{L}}}r^{\alpha^{\mathrm{L}}}\right)^{-1}u^{\alpha^{\mathrm{NL}}}}du\right), \quad \left(0<r\le d_1\right). \qquad (79)
\end{aligned}$$

In order to evaluate (79), we define the following integral functions according to [15],

$$\begin{aligned}\rho_1(\alpha,\beta,t,d) &= \int_0^d \frac{u^\beta}{1+tu^\alpha}du \\ &= \left[\frac{d^{(\beta+1)}}{\beta+1}\right] {}_2F_1\left[1,\frac{\beta+1}{\alpha};1+\frac{\beta+1}{\alpha};-td^\alpha\right], \end{aligned} \tag{80}$$

and

$$\begin{aligned}\rho_2(\alpha,\beta,t,d) &= \int_d^\infty \frac{u^\beta}{1+tu^\alpha}du \\ &= \left[\frac{d^{-(\alpha-\beta-1)}}{t(\alpha-\beta-1)}\right] {}_2F_1\left[1,1-\frac{\beta+1}{\alpha};2-\frac{\beta+1}{\alpha};-\frac{1}{td^\alpha}\right], (\alpha>\beta+1), \end{aligned} \tag{81}$$

where ${}_2F_1[\cdot,\cdot;\cdot;\cdot]$ is the hyper-geometric function [15].

Our proof is completed by plugging (80) and (81) into (79).

Appendix D: Proof of Lemma 4

Following the same approach in Appendix C, it is straightforward to derive $\mathscr{L}_{I_r}\left(\frac{\gamma r^{\alpha^{\mathrm{NL}}}}{PA^{\mathrm{NL}}}\right)$ for UAS 1 in the range of $0<r\le x_1$ as

$$\begin{aligned}\mathscr{L}_{I_r}\left(\frac{\gamma r^{\alpha^{\mathrm{NL}}}}{PA^{\mathrm{NL}}}\right) &= \exp\left(-2\pi\lambda\int_{r_2}^{d_1}\left(1-\frac{u}{d_1}\right)\frac{u}{1+\left(\frac{\gamma r^{\alpha^{\mathrm{NL}}}}{PA^{\mathrm{NL}}}PA^{\mathrm{L}}\right)^{-1}u^{\alpha^{\mathrm{L}}}}du\right) \\ &\quad\times\exp\left(-2\pi\lambda\int_r^{d_1}\frac{u}{d_1}\frac{u}{1+\left(\frac{\gamma r^{\alpha^{\mathrm{NL}}}}{PA^{\mathrm{NL}}}PA^{\mathrm{NL}}\right)^{-1}u^{\alpha^{\mathrm{NL}}}}du\right) \\ &\quad\times\exp\left(-2\pi\lambda\int_{d_1}^{\infty}\frac{u}{1+\left(\frac{\gamma r^{\alpha^{\mathrm{NL}}}}{PA^{\mathrm{NL}}}PA^{\mathrm{NL}}\right)^{-1}u^{\alpha^{\mathrm{NL}}}}du\right). \end{aligned} \tag{82}$$

Similarly, $\mathscr{L}_{I_r}\left(\frac{\gamma r^{\alpha^{\mathrm{NL}}}}{PA^{\mathrm{NL}}}\right)$ for UAS 1 in the range of $x_1<r\le d_1$ can be calculated by

$$\begin{aligned}\mathscr{L}_{I_r}\left(\frac{\gamma r^{\alpha^{\mathrm{NL}}}}{PA^{\mathrm{NL}}}\right) &= \exp\left(-2\pi\lambda\int_r^{d_1}\frac{u}{d_1}\frac{u}{1+\left(\frac{\gamma r^{\alpha^{\mathrm{NL}}}}{PA^{\mathrm{NL}}}PA^{\mathrm{NL}}\right)^{-1}u^{\alpha^{\mathrm{NL}}}}du\right) \\ &\quad\times\exp\left(-2\pi\lambda\int_{d_1}^{\infty}\frac{u}{1+\left(\frac{\gamma r^{\alpha^{\mathrm{NL}}}}{PA^{\mathrm{NL}}}PA^{\mathrm{NL}}\right)^{-1}u^{\alpha^{\mathrm{NL}}}}du\right). \end{aligned} \tag{83}$$

Our proof is thus completed by plugging (80) and (81) into (82) and (83).

Appendix E: Proof of Lemma 5

Following the same approach in Appendix C, for UAS 1, it is straightforward to derive $\mathscr{L}_{I_r}\left(\frac{\gamma r^{\alpha^{\mathrm{NL}}}}{PA^{\mathrm{NL}}}\right)$ for UAS 1 in the range of $r>d_1$ as

$$\mathscr{L}_{I_r}\left(\frac{\gamma r^{\alpha^{\mathrm{NL}}}}{PA^{\mathrm{NL}}}\right) = \exp\left(-2\pi\lambda\int_r^{\infty}\frac{u}{1+\left(\gamma r^{\alpha^{\mathrm{NL}}}\right)^{-1}u^{\alpha^{\mathrm{NL}}}}du\right)$$
$$= \exp\left(-2\pi\lambda\rho_2\left(\alpha^{\mathrm{NL}},1,\left(\gamma r^{\alpha^{\mathrm{NL}}}\right)^{-1},r\right)\right), \quad (r>d_1), \tag{84}$$

where $\rho_2(\alpha,\beta,t,d)$ is defined in (30).

Our proof is thus completed with (84).

REFERENCES

[1] CISCO, "Cisco Visual Networking Index: Global Mobile Data Traffic Forecast Update," 2013–2018, Feb. 2014.

[2] D. López-Pérez, M. Ding, H. Claussen, and A. H. Jafari, "Towards 1 Gbps/UE in cellular systems: understanding ultra-Dense small cell deployments," submitted to IEEE Communications Surveys and Tutorials, Oct. 2014.

[3] 3GPP, "TR 36.872 (V12.1.0), Small cell enhancements for E-UTRA and E-UTRAN - Physical layer aspects," Dec. 2013.

[4] J. G. Andrews, F. Baccelli, and R. K. Ganti, "A tractable approach to coverage and rate in cellular networks," IEEE Trans. Commun., vol. 59, no. 11, pp. 3122–3134, Nov. 2011.

[5] M. Haenggi, *Stochastic Geometry for Wireless Networks*. Cambridge University Press, 2012.

[6] M. Haenggi, J. G. Andrews, F. Baccelli, O. Dousse, and M. Franceschetti, "Stochastic geometry and random graphs for the analysis and design of wireless networks," IEEE J. Sel. Areas Commun., vol. 27, no. 7, pp. 1029–1046, Sep. 2009.

[7] F. Baccelli, M. Klein, M. Lebourges, and S. Zuyev, "Stochastic geometry and architecture of communication networks," J. Telecommunication Systems, vol. 7, no. 1, pp. 209–227, 1997.

[8] H. Dhillon, R. Ganti, F. Baccelli, and J. Andrews, "Modeling and analysis of K-tier downlink heterogeneous cellular networks," IEEE J. Sel. Areas Commun., vol. 30, no. 3, pp. 550–560, Apr. 2012.

[9] S. Singh, H. S. Dhillon, and J. G. Andrews, "Offloading in heterogeneous networks: Modeling, analysis, and design insights," IEEE Trans. Wireless Commun., accepted.

[10] X. Zhang and J. G. Andrews, "Downlink cellular network analysis with multi-slope path loss models," arXiv:1408.0549 [cs.NI], 2014.

[11] T. Bai and R. W. Heath Jr., "Coverage and rate analysis for millimeter wave cellular networks," arXiv:1402.6430 [cs.NI], 2014.

[12] M. Ding, et al., "FLINT: system-level simulation for LTE," wnt.sjtu.edu.cn/flint/html/index.html.

[13] 3GPP, "TR 36.828 (V11.0.0): Further enhancements to LTE Time Division Duplex (TDD) for Downlink-Uplink (DL-UL) interference management and traffic adaptation," Jun. 2012.

[14] Spatial Channel Model AHG (Combined ad-hoc from 3GPP & 3GPP2), "Spatial Channel Model Text Description,"Apr. 2003.

[15] I.S. Gradshteyn and I.M. Ryzhik, *Table of Integrals, Series, and Products (7th Ed.)*, Academic Press, 2007.

[16] M. Ding and H. Luo, *Multi-point Cooperative Communication Systems: Theory and Applications*, Springer & Shanghai Jiao Tong University Press, 2013.

[17] R. L. Burden and J. D. Faires, *Numerical Analysis (3rd Ed.)*, PWS Publishers, 1985.